NASA CONTRACTOR REPORT

NASA CR-1466

NUMERICAL CALCULATIONS OF VISCOUS COMPRESSIBLE FLUID FLOW OVER A FLAT PLATE AND STEP GEOMETRY

by John G. Trulio, Leonard Walitt, and William J. Niles

Prepared by
APPLIED THEORY, INC.
Santa Monica, Calif.
for George C. Marshall Space Flight Center

NATIONAL AERONAUTICS AND SPACE ADMINISTRATION • WASHINGTON, D. C. • FEBRUARY 1970

NUMERICAL CALCULATIONS OF VISCOUS COMPRESSIBLE FLUID FLOW OVER A FLAT PLATE AND STEP GEOMETRY

By John G. Trulio, Leonard Walitt, and William J. Niles

Prepared under Contract No. NAS 8-11400 by Desc only
APPLIED THEORY, INC.
Santa Monica, Calif.

for George C. Marshall Space Flight Center

NATIONAL AERONAUTICS AND SPACE ADMINISTRATION

For sale by the Clearinghouse for Federal Scientific and Technical Information
Springfield, Virginia 22151 – Price $3.00

TABLE OF CONTENTS

1.0	INTRODUCTION		
	1.1	Purpose	1
	1.2	Technical Approach	1
	1.3	Summary of Results	5
2.0	CALCULATIONS MADE AND RESULTS OBTAINED		7
	2.1	Summary of Problems Run	7
	2.2	Boundary Conditions	7
	2.3	Subsonic Laminar Flow Over a Flat Plate	9
	2.4	Axially Symmetric Step Calculations	12
	2.5	Supersonic Flat Plate Calculations	14
	2.6	Channel Calculations	21
3.0	CONCLUSIONS AND RECOMMENDATIONS		25
Tables			28
Figures			29
References			66

1.0 INTRODUCTION

1.1 Purpose of the Program

The main program objectives were: a) to determine the accuracy of the numerical methods embodied in the AFTON 2P computer code[1] in a calculation of subsonic laminar boundary layer flow over a flat plate, and b) assuming a successful flat plate calculation, to test the feasibility of using the AFTON 2A and AFTON 2P codes to compute supersonic and turbulent flow fields.

1.2 Technical Approach

The computer code AFTON 2P was applied to the specific problem of flow over semi-infinite flat plate at a Mach number of 0.2 and a Reynolds number per centimeter of 3.2×10^4. As a test of the AFTON 2P code, this problem presented the advantage that exact solutions are known[2] both for steady laminar flow over a semi-infinite plate, and for laminar boundary layer growth on an infinite flat plate; until perturbed by signals from the plate edge, boundary layer development aft of the plate's leading edge proceeds exactly as if the plate were infinite. For this subsonic plate flow problem, the question of the applicability of AFTON 2P centered on the use of very long, thin Eulerian cells in the calculation.[3] Earlier work had shown that boundary layer growth could be described by AFTON 2P with sufficient accuracy for most purposes, if one used finite difference cells whose width was less that that of the boundary layer by a factor of about four, or more. However, laminar flow over a semi-infinite flat plate results in a boundary layer whose thickness at any given distance from the plate's leading edge is much smaller than that distance itself. Hence, the use of square cells with edge lengths of only a fraction of the

boundary layer thickness would have led to the calculation of flow variables at an enormous number of finite difference mesh points, and to corresponding impractically high computation costs. On the other hand, the use of cells with the large length-to-width ratio ("aspect ratio") appropriate to a flat plate boundary layer, has led to large numerical inaccuracies in some past AFTON 2P calculations of continuum motion. The other aspects of the calculation of greatest interest also related to cell size, especially near the plate's leading edge where the entire boundary layer would be negligibly thick compared to any cell edge length that might be used in practice. Of particular concern were the effects of numerical leading edge inaccuracies on the flow field computed downstream, and on the bow shock which resulted from the assumed impulsive initial conditions.

While subsonic laminar flow afforded a necessary test of AFTON 2P, the main goal of the work reported here was seen initially as that of determining whether the AFTON 2A code could adequately calculate supersonic flow over an axisymmetric step; the specific step geometry programmed into AFTON 2A was taken from a Saturn V configuration provided by the sponsoring agency. However, by the time the calculation of step flow had proceeded through some of the early flow phenomena arising from impulsive initial conditions, it was clear that the real problem faced by AFTON 2P was not that of calculating supersonic flow, but of calculating the turbulent boundary layer known experimentally to form under the given flow conditions. No prior AFTON calculations of turbulent boundary layer flow had been made; in fact, to our knowledge the equations of continuum motion had not been integrated successfully for turbulent flow by any computer code. It was therefore decided that turbulent boundary layer

growth be isolated from the overall problem of flow around the Saturn V step, and the step flow calculation was accordingly separated into two parts.

The first of the two Saturn V problems was that of computing turbulent bounary layer growth forward of the almost-stationary shock created in the flow field by the step. Forward of the step, the radius of the Saturn body through most of its length was large compared to the anticipated maximum boundary layer thickness. Hence, the cylindrical surface was replaced for the boundary layer calculation by a flat plate; a leading-edge shock was thereby substituted for the shock attached to the nose of the cylinder. The second part of the step problem was then to compute flow over the step, starting a short distance upstream of the step shock. The boundary layer profile obtained in the turbulent flat plate calculation was to be used as an upstream boundary condition, and the flow field was to be computed for a distance of about 20 step heights downstream of the step.

From estimates of the rate of growth of eddies based on linear stability theory,[4] it was known beforehand that to carry out a definitive test calculation of turbulent flow over a flat plate would have been prohibitively expensive for this program, and that cells of practical size would give a necessarily coarse picture of the flow. Thus, although the calculation was worth trying, its results proved inconclusive. As a result, a search was begun for a set of flow field conditions which would lead to turbulent flow in a relatively short characteristic time and over relatively small characteristic distances, with the aim in mind of finding a definitive test of the code's ability to calculate the turbulence, at the

least possible cost. The problem finally selected and run for this purpose was that of turbulent plane-symmetric flow over a right circular cylinder in a narrow duct. While the calculation should be continued beyond the point to which it was taken in this program, the behavior of the flow field was markedly different from the laminar vortex fields previously successfully calculated, and strongly resembled that observed in turbulent wakes.

1.3 Summary of Results

The principal results of the program were as follows:

a) In the case of subsonic flow over a flat plate, laminar boundary layer profiles agreed well with exact solutions, both for the infinite flat plate and for steady flow over a semi-infinite plate. With the moderately dense meshes used (a maximum of 9 or 10 cells in the boundary layer), the numerical and exact velocity profiles differed by no more than about 7 percent. Furthermore, the transition between the two solutions was computed in considerable detail at many distances from the leading edge of the plate.

b) For the axisymmetric step with impulsive initial conditions, bow shock formation was computed up to the point where the shock front had moved about one step-width forward of the step itself, along with the associated flow field as it turned to accommodate the step.

c) The calculation of supersonic flow over a flat plate resulted in accurate leading-edge shock formation, with a laminar boundary layer below the shock. Further downstream the flow remained laminar for the mathematically plane plate of the problem. The introduction of irregularities on the plate surface near the leading edge, in an attempt to produce a turbulent boundary layer, did result in decidedly nonlaminar flow downstream, although it was not possible to determine whether the results represented numerical solution error, or a true numerical description of turbulence.

d) The calculation of flow over a wire trip in a duct employed a mesh fine enough to give a detailed picture of the boundary layer on the trip. A vortex formed on the back side of the trip, and shed. A second

vortex then grew in place of the first, reaching about one-third of the maximum diameter attained by the first vortex. At that stage in its development, the second vortex dissolved, leaving a region of small random-appearing velocities, closely simulating the breakup of vortices as it often (if not typically) occurs in the early stages of turbulent wake formation.

2.0 CALCULATIONS MADE AND RESULTS OBTAINED

2.1 Summary of Problems Run

The six problems run in the program were designated Problem 600.0, Problem 158.0, Problem 560.0, Problem 560.2, Problem 2.0, and Problem 561.0. They are described briefly in Table 1. In every case, air was treated as a polytropic gas ($\gamma = 1.4$) and was assumed to flow adiabatically. In Problem 600.0, subsonic flow was calculated over a flat plate, while in Problems 158.0, 560.0, and 560.2 supersonic flat plate flow was calculated. Problem 2.0 was concerned with supersonic flow over an axially symmetric step. In Problem 561.0, viscous compressible flow was calculated over a wire trip in a plane, two-dimensional channel, under conditions which would result in Poiseuille flow in the absence of the trip.

2.2 Boundary Conditions

In Problems 600.0, 158.0, 560.0, 560.2, and 2.0, the density, energy, and velocity of material at the upstream boundary were given their free stream values. The upstream boundary conditions for Problem 561.0 consisted of a velocity profile characteristic of steady, fully developed plane Poiseuille flow in a channel,[5] a specific energy profile from the isoenergetic relation[5] (which was assumed valid at the upstream boundary), and a density profile from the energy profile and the perfect gas law, i.e.,

$$P = (\gamma - 1)\ \rho\ E \qquad (1)$$

where P is the pressure, E is the specific internal energy, ρ is the density, and γ is the ratio of specific heats. The pressure in Equation (1) was assumed constant along the upstream boundary.

The downstream boundary condition used in all the AFTON 2P and AFTON 2A problems reported here is based largely on characteristic theory; details have been presented in previous reports.[3,7] The same condition was employed in our previous cylinder studies[3,7] and appeared to provide a good approximation to flow at the downstream boundary.

A no-slip rule was enforced at the surface of each obstacle, while the fluid was allowed to slide without friction at the system's lateral boundaries, i.e., at a lateral boundary, the normal component of velocity, and the tangential stress, were zero.

2.3 Subsonic Laminar Flow Over a Flat Plate

A study was made of subsonic laminar flow over a flat plate at a free stream Mach number of 0.20 and a Reynolds number per centimeter of 3.2×10^4 (Problem 600.0). An Eulerian finite difference mesh consisting of 2912 mesh points was used in the calculations. Problem 600.0 was run from impulsive initial conditions, i.e., a uniform velocity, density, and energy were imposed throughout the flow field at zero time, except for the no-slip condition at the plate surface. In order to obtain the leading edge solution, the upstream boundary was located normal to the plate at 0.10 cm upstream of the plate's leading edge. The downstream boundary was located normal to the plate 18 cm from the plate's leading edge. The lateral boundary, where frictionless flow was enforced, was made parallel to the plate at 0.593 cm from the plate surface. Thus, the flow studied was that in the entrance to a channel of height 1.186 cm.

Various stages in the development of the plate flow are illustrated in the velocity vector plots of Figures 1, 2, and 3. The vectors in the figures are proportional to the particle velocities at the points of the finite difference mesh; a mesh point is located at the tail of each vector. In Figure 1, the velocity field is shown at an early stage of motion. Figure 2 clearly exhibits the growth of the initial vortex sheet at the plate surface at a somewhat later time, when free stream particles have traveled 0.68 plate lengths.

From a study of the velocity field of Figure 2, it was found that the profiles over most of the downstream portion of the plate were independent of distance along the plate surface. Hence, at this particular

time the flow field approaches that of a viscous fluid over an infinite flat plate (Rayleigh Problem). The velocity profile at a station corresponding to 0.72 plate lengths from the plate leading edge (Station 1.695×10^{-4} KM, see Figure 2) was compared to the Rayleigh solution.[8] The results are presented in Figure 4, where the ratio of local to free stream velocity, U/U_∞, is plotted as a function of the Rayleigh similarity parameter $\eta = y/2\sqrt{\nu t}$; here y is distance normal to the plate, t is the time, and ν is the kinematic viscosity. The data used to prepare Figure 4 were generated by AFTON 2P at various stages of the motion, up to a time corresponding to 0.72 plate lengths of travel by a free stream particle. The numerical results differ from the infinite plate solution by less than 5 percent; most of the difference is believed to result from the proximity of the lateral boundary to the plate, whereas the Rayleigh solution applies to an infinitely wide channel.

From a study of the velocity profiles of Problem 600.0 at times later than those of Figure 4, but at the same station, it was found that a transition from the Rayleigh solution to the steady-state semi-infinite channel solution (steady flow in the entrance to a channel) occurred at a time corresponding to 0.72 plate lengths of travel by a free stream particle. Hence, in the time required for a free stream particle to travel from the plate leading edge to a particular downstream station, a transition is made at that station, from Rayleigh flow, to steady flow in a semi-infinite channel.

In Figure 3, laminar boundary layer velocity profiles can be seen at a time late enough so that steady-state flow has nearly been achieved. It can also be seen in Figure 3 that the velocity vectors

oscillate in the neighborhood of the plate leading edge. These oscillations are believed to be numerical rather than physical, resulting from deceleration of the flow from Mach 2.0 to zero in one zone along the dividing streamline at the plate leading edge. The calculated steady-state velocity profile 0.72 plate lengths aft of the leading edge was compared to Schlichting's solution for flow in the entrance to a channel.[9] The results are presented in Figure 5, along with the Blasius solution for flow over a semi-infinite flat plate;[10] position normal to the plate at a given downstream station is indicated by the Blasius similarity parameter $\eta = y\sqrt{U_\infty/\nu x}$ . . Although the numerical velocity profile is still slowly approaching a true steady state, the numerical results differ from the Schlichting solution by less than 7 percent.

2.4 Axially Symmetric Step Calculations

The flow over an axisymmetric 90^{o} step (Problem 2.0) was investigated using the AFTON 2A computer code, which integrates numerically the equations of two-dimensional transient axisymmetric continuum motion. The body configuration of Problem 2.0 was taken from a portion of a Saturn test model which was experimentally investigated at the Marshall Space Flight Center. The outer radius of the step was .7 in. and the inner radius was 5 in. The complete Saturn test model configuration is shown in Figure 6. The finite difference mesh utilized for this study was composed of 3080 mesh points with an upstream boundary located 10 in. forward of the step (Station -10, see Figure 6) and a downstream boundary located 9.5 in. aft of the step (Station 9.5 in., see Figure 6). The lateral boundary of the mesh was located 15.5 in. from the axis of the body. The free stream Mach number was 1.5, and the free stream Reynolds number was 2.8×10^{6} per foot. Uniform free stream conditions were imposed at the upstream boundary of the mesh and impulsive initial conditions were used to start the problem.

The development of the bow shock which recedes from the step, is illustrated in the velocity vector plots of Figures 7 and 8. Figure 7 gives the impulsive initial flow field, while flow over the axisymmetric step is shown in Figure 8 at an early stage of motion (characteristic time[≠]

[≠]The characteristic time is defined as the number of step heights that a particle traveling with free stream velocity would move in a given time.

of 7.85). In Figure 8, the bow shock can be seen receding from the step. Downstream of the bow shock, velocity oscillations are evident which are similar to those found in a region of turbulence. Although Problem 2.0 has not been run much beyond a characteristic time of 1.57, the behavior of the flow field agrees at least qualitatively with available experimental results;[11] turbulent oscillations have been observed in the separated region between the bow shock and the step.

Since a bow shock is a permanent feature of the flow field of Problem 2.0, it seems appropriate to discuss briefly here the treatment of shocks in the AFTON 2A code. The AFTON 2A equations are basically Lagrangian, and in most numerical analogs of the equations of motion in Lagrangian form, shock waves are not computed as discrete discontinuities. Instead, dissipative stresses are introduced which cause the mathematical surfaces of discontinuity to be replaced by thin layers in which the pressure, density, temperature, etc., vary rapidly but continuously. For flows which are ideally inviscid, the AFTON codes presently employ an artificial viscosity function developed by von Neumann and Richtmyer[12] to effect shock transitions; with this dissipation function, it can be shown that the equations of motion are consistent with the Rankine-Hugoniot equations. In the case of viscous flow, dissipative stresses are an essential element in the formulation of the equations of motion, and it was not found necessary to use an artificial dissipation function either in the axisymmetric flow calculations discussed above, or in the flat plate calculations discussed in Section 2.5. It is evident from Figure 8 that the variables of the motion nevertheless changed quite abruptly in the neighborhood of the bow shock of Problem 2.0.

Problem 2.0 was primarily a pilot problem designed to test the AFTON 2A code for axisymmetric viscous flow, and it was therefore of minor concern that the uniform upstream boundary condition imposed in the problem is not physically correct. Actually, the flow upstream of the Saturn test model step is influenced by the forebody geometry. In order to account for the effects of the forebody, a problem of flow over a flat plate first had to be run; the flat plate flow field at a distance from the plate edge equal to the length of the forebody would then serve as boundary condition data for the axisymmetric step (see Section 1.2).

2.5 Supersonic Flat Plate Calculations

In order to generate boundary data for the axisymmetric step problem, flow over a flat plate was numerically investigated at a free stream Mach number of 2.0 and at a Reynolds number per foot of 3.48×10^6. The velocities, densities, and energies at a distance of 0.75 plate lengths from the leading edge (Station -16, Figure 6) were recorded for this purpose in each of three flat plate calculations.

First, a problem designated as Problem 158.0 was started from impulsive initial conditions, with a finite difference mesh consisting of 4200 points in a rectangular array. The points were separated by uniform increments of 0.04 ft along the plate surface, and .008 ft normal to the plate. The plate for Problem 158.0 was 5.92 ft long. At the axial station -16 in. (see Figure 6), a turbulent boundary layer would then have a thickness equal to about 6 cell widths. In Problem 158.0, a lateral boundary was placed parallel to the plate surface at a distance of 0.388 ft. The inlet boundary in Problem 158.0 was 0.04 ft upstream of the plate leading edge with one zone between the leading edge and the

upstream boundary. A triangular trip was placed on the plate surface at a distance of 0.287 ft from the plate leading edge. The trip height of .003 ft is equal to 80 percent of the laminar boundary layer thickness at this position.

The second problem run in this numerical investigation was Problem 560.0. Problem 560.0 was similar to Problem 158.0, but the inlet boundary was moved 0.1 ft upstream of the plate leading edge, and 12 zones were put between the leading edge and upstream boundary. Problem 560.0 also had closer mesh point spacing normal to the plate than did Problem 158.0, the minimum increment in Problem 560.0 being .006 ft. A triangular trip was placed on the plate surface at a distance of .663 ft from the plate leading edge in this problem. Finally, in Problem 560.2, five triangular trips replaced the lone trip of Problem 560.0.

A velocity vector plot of a plate flow field obtained in Problem 158.0 is presented in Figure 9, at a time when free stream particles have traveled .49 plate lengths. Since the inlet boundary was placed upstream of the plate leading edge, the effect of the leading edge on the flow can be seen. At the Reynolds number for the problem the flow should become turbulent, and random oscillations are, in fact, seen in the velocity vectors near the plate surface starting from the plate leading edge. The trip is also indicated in Figure 9. The average boundary layer velocity profile was computed at a distance of $.155^5$ plate lengths from the plate leading edge. The resulting profile is presented in Figure 10, along with velocity profiles obtained from the 1/7 power law[13] of turbulence, and from Crocco's flat plate laminar boundary layer solution at Mach 2.0.[14] It can be seen from Figure 10 that the calculated average velocity profile is much closer to a 1/7 power law, than is

the Crocco profile. In fact, the calculated average velocity profile approximates a 1/5 power law. In Figure 9, it can be seen that the plate leading edge not only produces a shock wave, but also seems to be the source of the "turbulent" oscillations. It is believed that deceleration of the flow from Mach 2.0 to zero in one cell width along the dividing streamline at the plate leading edge, is the primary cause of the oscillations. As noted in Section 2.3, similar fluctuations were observed for subsonic flow over a flat plate.

The flat plate results of Problem 158.0 were encouraging. However, a conclusive demonstration that turbulence can be calculated directly from the conservation principles of classical mechanics, would exhibit the process of transition from laminar to turbulent flow. With this objective in mind, Problem 158.0 was rerun with a finer finite difference mesh in the neighborhood of the plate leading edge, so that greater accuracy might be obtained in describing the leading edge shock wave, and subsequent laminar boundary layer growth near the leading edge. In order to induce transition to turbulence, a triangular trip was placed on the plate surface at a station corresponding to a Reynolds number of 2.0×10^6. The trip height was made equal to the laminar boundary layer thickness at this station, and the trip width was 6.35 laminar boundary layer thicknesses.

For Problem 560.0, the finite difference mesh was composed of 6683 mesh points, and is shown in Figure 11; impulsive initial conditions were employed in the problem. A velocity vector plot of the flow field of Problem 560.0 is presented in Figure 12. An oblique shock front, and a laminar flow field below it, are seen in the neighborhood of the plate leading edge. As Figure 12 shows, the change in flow properties across

the oblique shock front at the plate leading edge, was more gradual in Problem 560.0 than for the axisymmetric step (Problem 2.0; see Section 2.4). In the neighborhood of the plate leading edge (where the density of mesh points is greatest), the shock front was approximately four zones thick. As in the case of axisymmetric flow, the flat plate calculations were made without introducing an artificial dissipation function.

The angle between the leading edge shock and the plate of Problem 560.0, was compared to the corresponding angle calculated from a combination of boundary layer theory and the jump conditions across oblique shocks. A shock angle of 32.9^{o} relative to the plate was estimated from the velocity vector plot of Figure 12, as an average of the angles between the plate and each of two straight lines which approximately bound the oblique shock region. An independent estimate of the angle of the leading-edge shock was obtained, assuming that the boundary layer near the plate leading edge effectively converts the plate to a wedge, which causes the free stream flow to turn by means of an oblique shock. Accordingly, the angle of the shock above a given point of the boundary layer surface, was computed as that due to a wedge with a slope equal to the derivative of the displacement thickness, δ^*, with respect to distance,y,parallel to the plate[15]. The Stewartson transformation[16] was employed to determine a boundary layer displacement thickness for compressible flow, using the momentum thickness, θ_i, and displacement thickness, δ_i^*, of an equivalent incompressible flow. For the adiabatic flow of a gamma-law gas over a flat plate with Prandtl number unity, the pertinent relationships are as follows:

$$\delta^* = \left(\frac{P_s}{P_\infty}\right)^{\frac{\gamma+1}{2\gamma}} \left[1+\frac{\gamma-1}{2} M_\infty^2 \left(1+\frac{\theta_i}{\delta_i^*}\right)\right] \delta_i^* \qquad (2)$$

$$\theta_i = \frac{.664y}{\sqrt{R_{ei}}} \left(\frac{\rho_\infty}{\rho_s}\right)\sqrt{\frac{T_\infty}{T_s}} \left(\frac{\mu_\infty}{\mu_s}\right) \tag{3}$$

$$\delta_i^* = \frac{1.72y}{\sqrt{R_{ei}}} \left(\frac{\rho_\infty}{\rho_s}\right)\sqrt{\frac{T_\infty}{T_s}} \left(\frac{\mu_\infty}{\mu_s}\right) \tag{4}$$

$$R_{ei} = \frac{\rho_\infty U_\infty y}{\mu_\infty} \sqrt{\frac{T_\infty}{T_s}} \left(\frac{\mu_\infty}{\mu_s}\right) \tag{5}$$

where R_{ei} is the Reynolds number for the equivalent incompressible flow, M_∞ is the free stream Mach number, U_∞ is the free stream velocity, T_∞ is the free stream temperature, T_s is the free stream stagnation temperature, P_∞ is the free stream pressure, P_s is the free stream stagnation pressure, ρ_∞ is the free stream density, ρ_s the free stream stagnation density, μ_∞ is the free stream viscosity, and μ_s is the free stream stagnation viscosity. The leading edge shock angle, β, is then determined from the oblique shock equations[17], where the effective wedge angle θ is given by

$$\theta = \tan(\delta^*/y) \tag{6}$$

In the present case, the distance y was taken as .1 ft from the leading edge of the plate. At this distance the oblique shock produced in Problem 560.0 is clearly visible in Figure 12; at the same time, the bow shock near the tip of the plate, where the parabolic boundary layer surface meets the plate edge at a right angle, is of insignificant dimension compared with .1 ft. On this basis, the angle of the oblique shock calculated from Equations (2)-(6) and the oblique shock transition equations, differed from that of Problem 560.0 by 4.5%.

Downstream of the leading-edge shock of Problem 560.0, in the neighborhood of the trip, oscillations are seen in the velocity vectors of Figure 12; however, they appeared to damp out a short distance aft of the trip. The frequency of the disturbance introduced by the trip was evaluated relative to measurements of neutral stability made by Schubauer and Skramstad[18] on a subsonic flat plate at zero incidence (see Figure 13), and the the numerical stability calculations of Mack[19] for a flat plate at Mach 2.2 (see Figure 14). The disturbance frequency due to the trip is seen to lie in the damped region of the neutral stability curves for both the subsonic and supersonic plate flows. Thus, the leading edge phenomena calculated numerically were qualitatively correct for this case, and a disturbance of greater amplitude and frequency is necessary to induce transition to turbulence.

In order to increase the amplitude and frequency of the input disturbance, five trips (each of height 2.0 laminar boundary layer thicknesses and width 2.67 laminar boundary layer thicknesses) were introduced at a station corresponding to a Reynolds number of 2.0×10^6 (Problem 560.2). The finite difference mesh in Problem 560.2 is shown in Figure 5. Velocity vector plots of the computed flow field are presented in Figures 16 and 17 at times when the free stream particles have moved .245 plate lengths and .452 plate lengths, respectively. Random oscillations are seen propagating downstream in the wake behind the trip region. The frequency of the disturbance introduced by the trips is also compared to the experimental data of Schubauer and Skramstad and the numerical data of Mack (see Figures 13 and 14). It is seen that the disturbance frequency introduced by the trips is within the unstable region bounded by the neutral

stability curves for both the subsonic and supersonic plate flows. Hence, it was believed that the disturbance produced in the trip region would cause transition to turbulence. However, upon further running of Problem 560.2, it was found that the amplitude of the disturbance introduced by the trip continually damped as time progressed. Thus, steady-state laminar flow over a flat plate (with a trip) was approached, instead of turbulent flow over a flat plate.

Experimentally[20] it has been shown that vortices, which continally form and shed behind a trip, are the primary source of the perturbations which cause transition to turbulence. Study of the numerical flat plate flow field data indicated that no vortices had developed in the region behind the trip. Since the AFTON 2P computer code is capable of calculating vortices behind an obstacle if a sufficiently fine mesh is used[3,7], it was concluded that for the problem at hand, the mesh points were too widely spaced in the vicinity of the trip; in order to compute vortices behind the trip, and the subsequent transition to a turbulent boundary layer, a greater mesh point density than that of Problem 560.2 is needed in the neighborhood of the plate surface and the trip.

2.6 Channel Calculations

In order to define the vortices which form and shed behind a trip in greater detail than was practical in the supersonic flat plate problem, it was decided to investigate numerically fully developed plane Poiseuille flow in a two-dimensional channel, rather than to recompute Problem 560.2 with a finer mesh. Fully developed channel flow changes the scale of the problem so that the entire region of calculation lies within the boundary layer. In the supersonic plate problem, the boundary layer constituted about 5 percent of the flow field. Thus, 30 points could be obtained in the boundary layer in the channel problem instead of the 4 points which defined the boundary layer profiles in the supersonic flat plate problem. It was felt that success in calculating the transition from laminar to turbulent flow in a channel would demonstrate conclusively that turbulent flow fields can be computed directly from the conservation principles of classical mechanics. Then, with finer meshes than those used in Problems 560.0 and 560.2, we would expect to calculate turbulence on the supersonic flat plate.

The channel flow study (Problem 561.0) was conducted at an average Reynolds number of 10,000 based on the channel height and average velocity at the channel entrance. This is about twice the experimentally measured critical Reynolds number for transition from laminar to turbulent flow in a channel. A wire trip was placed on the top and bottom walls of the channel at a distance of .858 channel heights from the channel entrance. The wire trip was sized so that transition would occur immediately downstream

of the trip. According to the experimental results of Fage and Preston[21] the minimum height for which transition occurs at the trip element itself can be found from the relation

$$\frac{U_\tau^* K_{crit}}{\nu} \geq 20 \tag{7}$$

where:

$U_\tau^* = \sqrt{\tau_w/\rho}$

τ_w, wall shear stress

ρ, density

K_{crit}, critical trip height

ν, Kinematic viscosity

From the fully developed laminar channel solution[22]

$$U_\tau^* = \sqrt{6}\ \ \overline{U}/\sqrt{R_D} \tag{8}$$

where:

$\overline{U}$, average velocity at channel entrance

$R_D = \frac{\overline{U}D}{\nu}$

D, channel height

Combination of Equations (7) and (8) yields

$$\frac{K_{crit}}{D} \geq \frac{20}{\sqrt{6}\ \ \sqrt{R_D}} \tag{9}$$

For R_D = 10,000, we obtain K_{crit}/D = .0818. However, to insure an effective trip in this numerical study, K_{crit}/D = .14 was used.

The finite difference mesh for Problem 561.0 was developed from the streamlines and potential lines of the potential theory solution for flow over a wire trip.[23] The finite difference mesh, which is composed of

4717 points, is shown in Figure 18. Since the channel centerline is an axis of symmetry, the lateral boundaries of the region of calculation consist of the channel centerline and the channel wall. The plane Poiseuille parabolic velocity profile[22] was imposed at the upstream boundary of the mesh. The average Mach number at the upstream boundary was 0.20. A no-slip condition was imposed along the plate and trip surfaces. Frictionless flow was required along the centerline of the channel, and the characteristic boundary condition employed previously[3,7] was imposed at the downstream boundary. The values of the flow field variables at the upstream boundary were used as initial values throughout the mesh.

So far, Problem 561.0 has been run to a characteristic time of 9.9[≠]. The initial impulsive flow field is shown in the velocity vector plot of Figure 19 (characteristic time of 0.0). The potential flow field solution about the trip is obtained during the early stages of motion (see Figure 20). At a characteristic time of 2.95, a vortex formed behind the trip. A velocity vector plot of this flow field is shown in Figure 21. Vortex shedding was initiated at a characteristic time of about 5.75 (see the velocity vector plot of Figure 22). A secondary vortex in an early formative stage, is also indicated in Figure 22. In Figure 23 (characteristic time of 8.75) the first vortex has moved downstream and the second vortex is well-formed behind the trip. Some random fluctuations are also indicated in the velocity vectors between the two vortices. At

[≠]The characteristic time (τ) corresponds to the number of trip heights of travel by a particle moving with the centerline velocity at the upstream boundary, i.e., $\tau = 1.5t\bar{U}/K_{crit}$.

a characteristic time of 9.9 (Figure 24), the first vortex continues to propagate downstream. However, the secondary vortex (or eddy) has dissolved and fluctuating velocities have replaced it. In previous vortex shedding problems[7] an eddy once formed grew into a vortex which shed. This is our first numerical calculation of the formation and disintegration of an eddy.

Schlichting[24] described turbulence in terms of portions of the fluid (eddies) having their own intrinsic motion superimposed on the main flow. The continual formation and disintegration of these eddies determines the scale of turbulence. Turbulent eddies were made visible by photographing turbulent flow in a water channel with varying camera speeds. Photographs of this kind were taken by Nikuradse,[25] and are presented in Figure 25. The numerical results of Problem 561.0 have duplicated the eddy formation and disintegration process characteristic of turbulence. Thus, it is believed that further running of Problem 561.0 will result in a calculation of the full transition from laminar flow to a two-dimensional analog of true three-dimensional turbulent flow.

3.0 CONCLUSIONS AND RECOMMENDATIONS

The results of the laminar plate calculations performed in this program, particularly for supersonic flow, provided further evidence of the ability of existing numerical techniques to give quantitatively useful descriptions of laminar flow fields; earlier calculations of laminar boundary layer formation on a right circular cylinder also showed excellent agreement with boundary layer profiles obtained by analytic methods. Furthermore, although in practice no finite difference mesh can provide detail within the boundary layer as the leading edge of the plate is approached, it appears that lack of definition near the leading edge does not affect the accuracy of a numerical flow field further downstream, where the boundary layer thickness is several times the distance between adjacent mesh points. In fact, even the leading edge shock was found to be accurately represented in the finite difference solution. We therefore conclude that as a practical matter, using existing numerical methods and computers, a wide and important class of laminar flows can be calculated numerically, even when finite difference cells of large aspect ratio (> 4) are employed in the process.

A further result of considerable theoretical interest is that shocks can be included in at least some viscous compressible supersonic flow problems without the need for an artificial viscosity. Pertinent examples in this program were the laminar plate leading edge shock, and the bow shock which recedes from an axisymmetric step under impulsive initial conditions. While it was not clear whether the flow field viscosity, and/or the discretization error, and/or the conservation

properties of the finite difference equations, were responsible for effecting the shock transition, the fact is that the transition was made. In future calculations of viscous compressible flow, we will therefore not introduce an artificial viscosity without fresh evidence of the need for it; it appears that the Rankine-Hugoniot equations will be satisfied anyway across an ambient shock.

An important negative result of the flat plate calculations reported here is that even the deliberate introduction of roughness, with an amplitude comparable to that of the boundary layer thickness, produced only decaying transients. Since the flow parameters were given values known to result in turbulent boundary layer formation, we must conclude either that a turbulent boundary layer on a plate cannot be calculated using the AFTON 2P code, or that the calculation requires a denser set of mesh points than that employed in this program; we are inclined to believe the latter, as noted below.

The calculation of flow over a trip in a narrow duct has provided the strongest evidence to date that the numerical methods embodied in codes like AFTON 2P are capable of providing a quantitative account of turbulent flow. This we consider the most important result of the group of calculations reported here. The fact that a test case had to be carefully selected to make even this limited demonstration possible, is at least partly offset by the order-of-magnitude reduction in computing costs which can be achieved by making use of recent advances in numerical methods and in computing hardware. By incorporating into the AFTON 2P code time-saving techniques already tested in small-scale calculations, and by

employing the most efficient computers presently available, it appears likely that a significant class of turbulent flow fields can be calculated numerically, including a turbulent boundary layer on a flat plate.

In future calculational programs of the kind discussed here, the highest priority should be assigned to carrying the trip-in-a-narrow-duct problem to as late a stage of development as is economically feasible. The importance of this problem in providing a definitive answer to the feasibility of AFTON 2P calculations of turbulence, outweighs the fact that the flow itself is quite special, and perhaps of little intrinsic interest. Of less urgency, but still highly desirable, is the incorporation of improved numerical techniques into the AFTON 2P code, and the adaptation of the code to the most efficient computers presently available, or soon to become operational. The potential reduction of computing costs for presently feasible calculations, and the potential enlargement of the class of calculable flows to be achieved thereby, justify considerable emphasis on these tasks. It is then recommended that proof of the gain in efficiency so obtained be exhibited in the form of a successful calculation of turbulent boundary layer formation on a flat plate. Assuming that the results of such a flat plate calculation are satisfactory, the calculation of flow over a step on a Saturn V missile should then be resumed because of its practical significance.

TABLE 1

SUMMARY OF PROBLEMS RUN

Problem Number	Reynolds Number	Time Step Increment	No. of Time Steps Run	Type of Upstream Boundary Condition	Type of Initial Condition	Dimensions of Finite Different Mesh
600.0	3.2×10^4 per cm	3×10^{-4} msec	0 - 14,000	Uniform Energy, Density and Velocity	Impulsive	16 x 182
158.0	3.48×10^6 per ft	1×10^{-6} sec	0 - 2,360	Uniform Energy, Density and Velocity	Impulsive	28 x 150
560.0	3.48×10^6 per ft	4×10^{-7} sec	0 - 1,500	Uniform Energy, Density and Velocity	Impulsive	41 x 163
560.2	3.48×10^6 per ft	4×10^{-7} sec	0 - 2,280	Uniform Energy, Density and Velocity	Impulsive	41 x 163
2.0	2.8×10^6 per ft	1×10^{-5} sec	0 - 1,500	Uniform Energy, Density and Velocity	Impulsive	35 x 88
561.0	1×10^4	6.125×10^{-4} msec	0 - 3,820	Velocity profile for plane Poiseuille flow, energy profile from isoenergetic relation, and density profile from perfect gas equation of state with constant pressure	Initial flow field that of steady plane Poiseuille flow	30 x 157

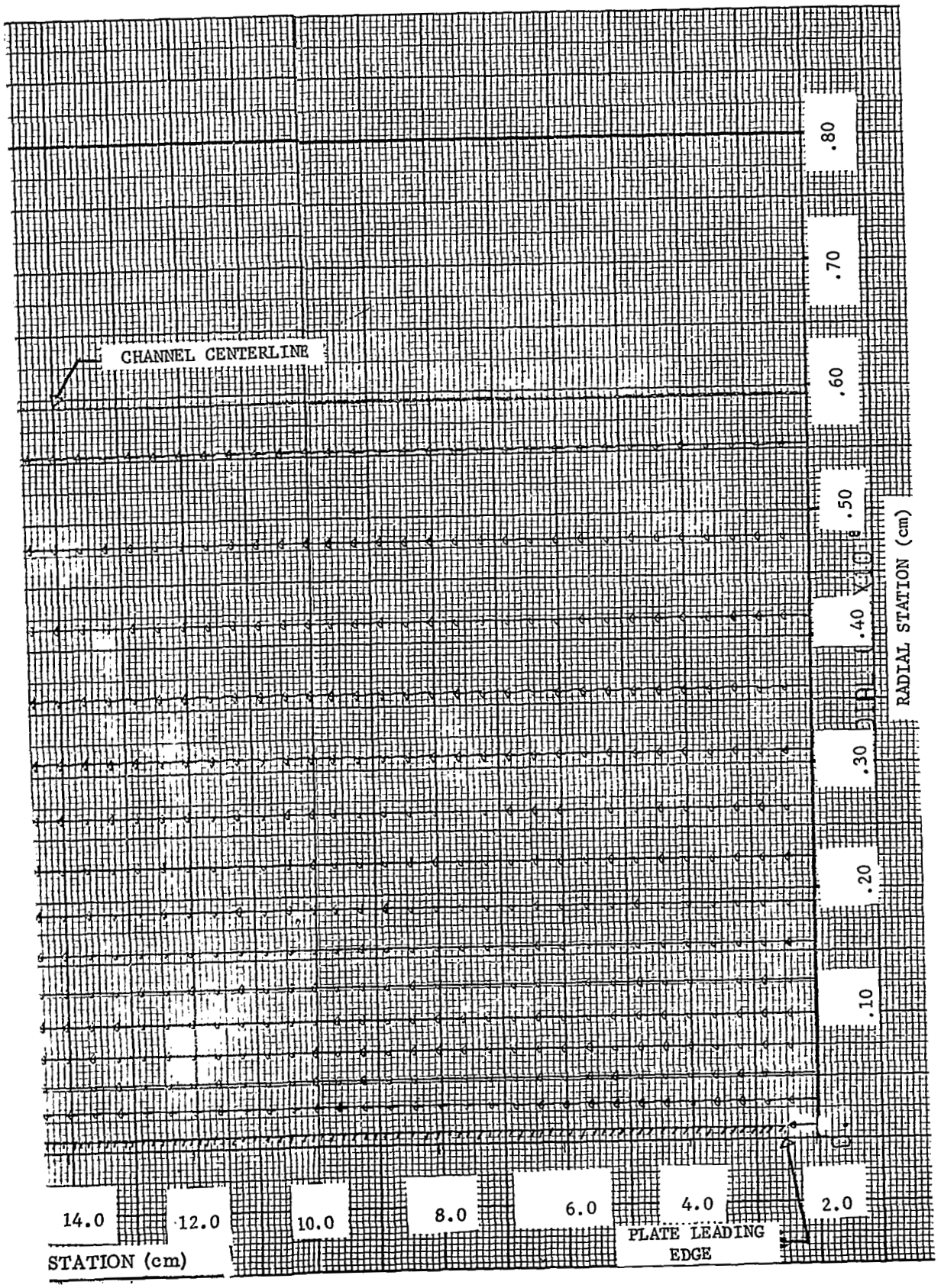
CHANNEL CENTERLINE
.80
.70
.60
.50
.40
.30
.20
.10
RADIAL STATION (cm)
14.0
12.0
10.0
8.0
6.0
4.0
2.0
PLATE LEADING EDGE
STATION (cm)

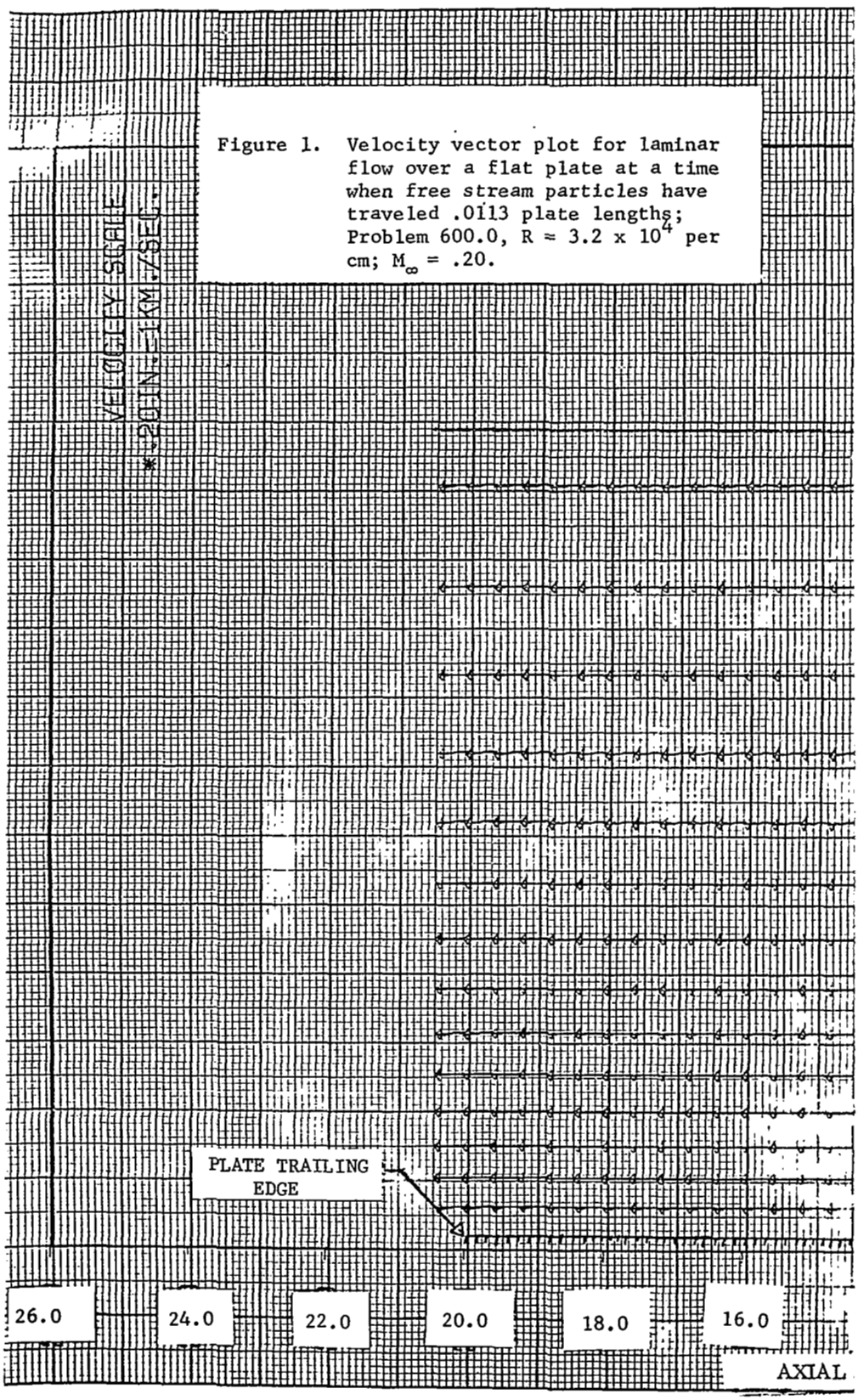

Figure 1. Velocity vector plot for laminar flow over a flat plate at a time when free stream particles have traveled .0113 plate lengths; Problem 600.0, $R \approx 3.2 \times 10^4$ per cm; $M_\infty = .20$.

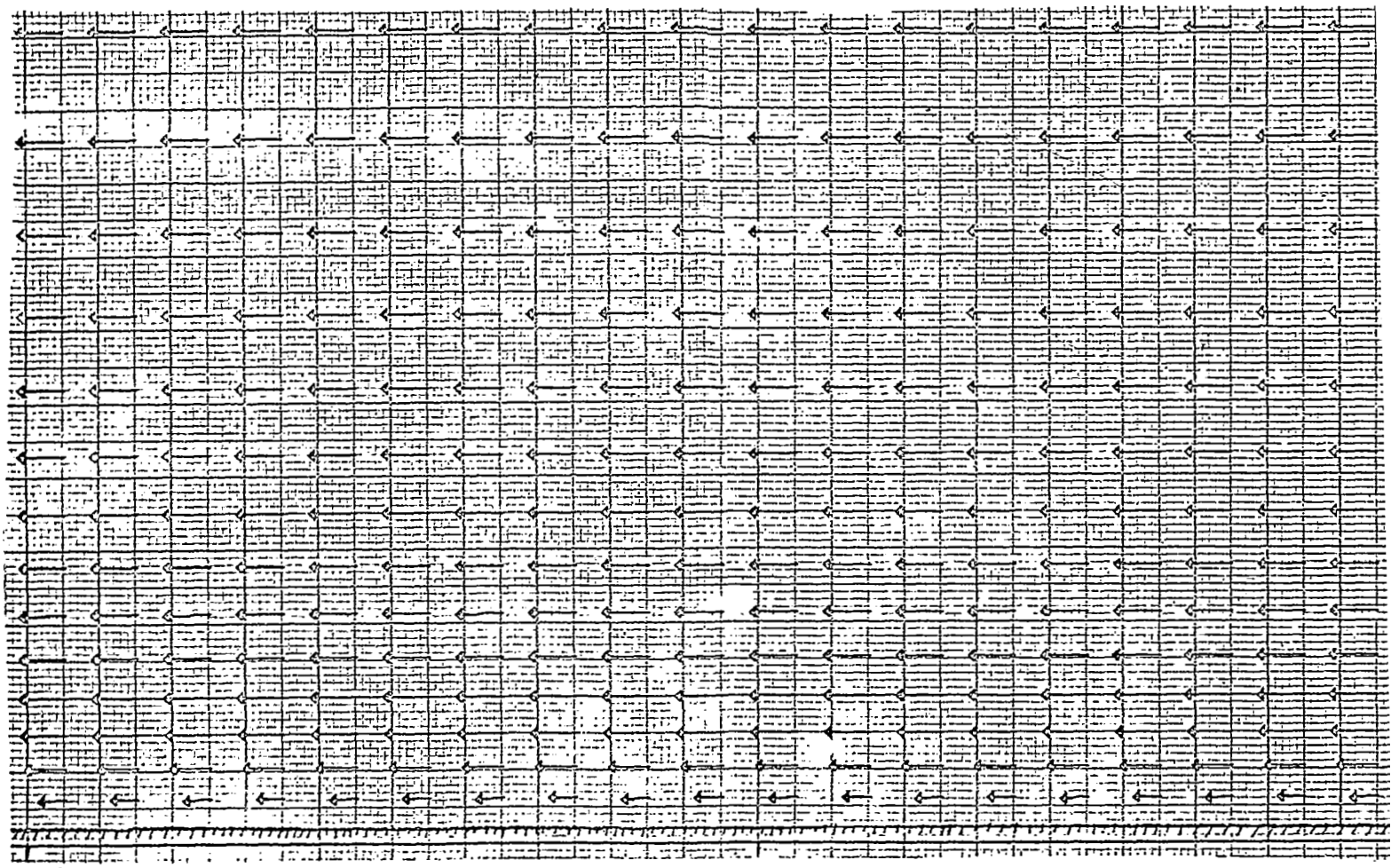

18. 17.

AXIAL STATION (cm)

Figure 2. Velocity vector plot for laminar flow over a flat plate at a time when free stream particles have traveled .68 plate lengths; Problem 600.0, $R = 3.2 \times 10^4$ per cm; $M_\infty = .20$.

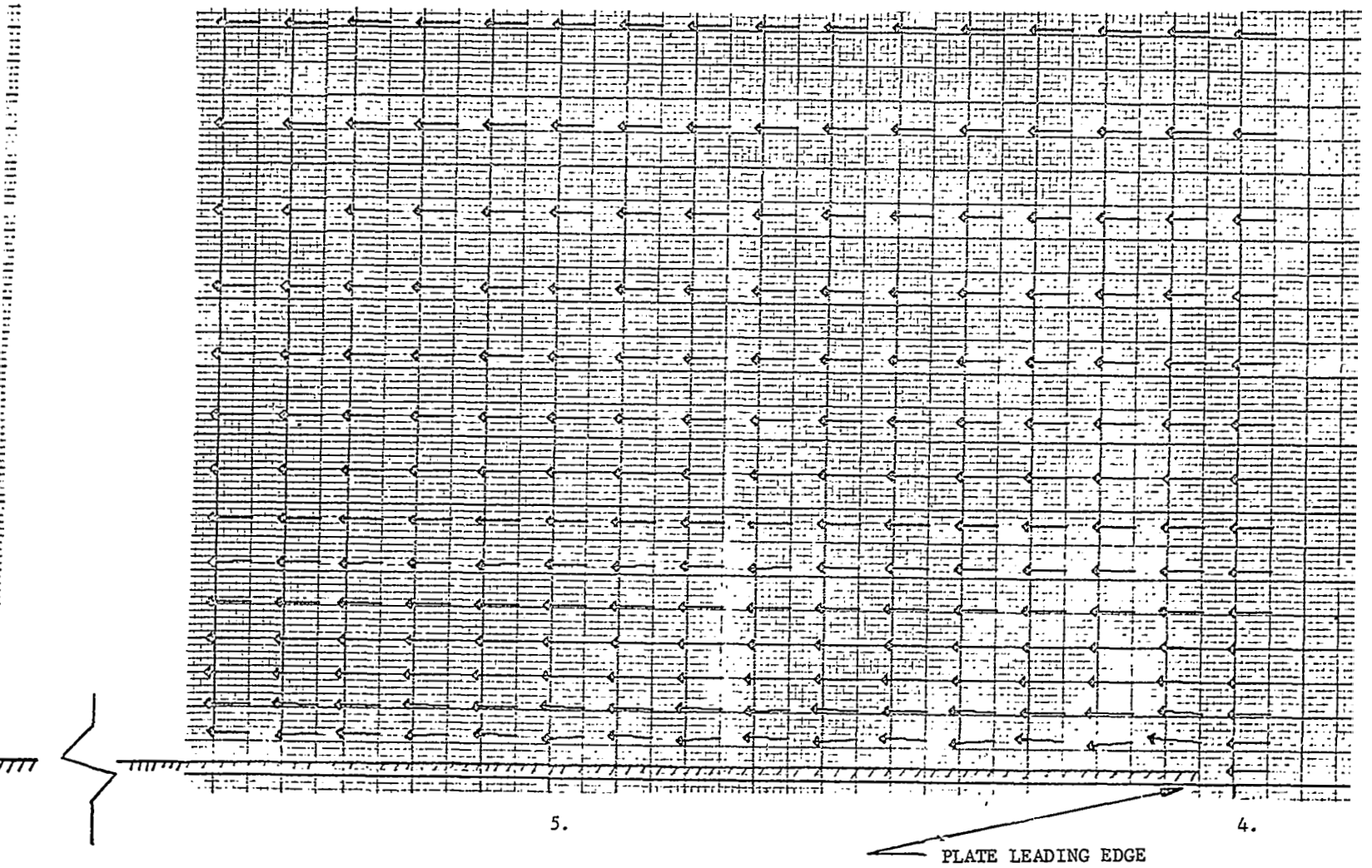
5.
4.
PLATE LEADING EDGE

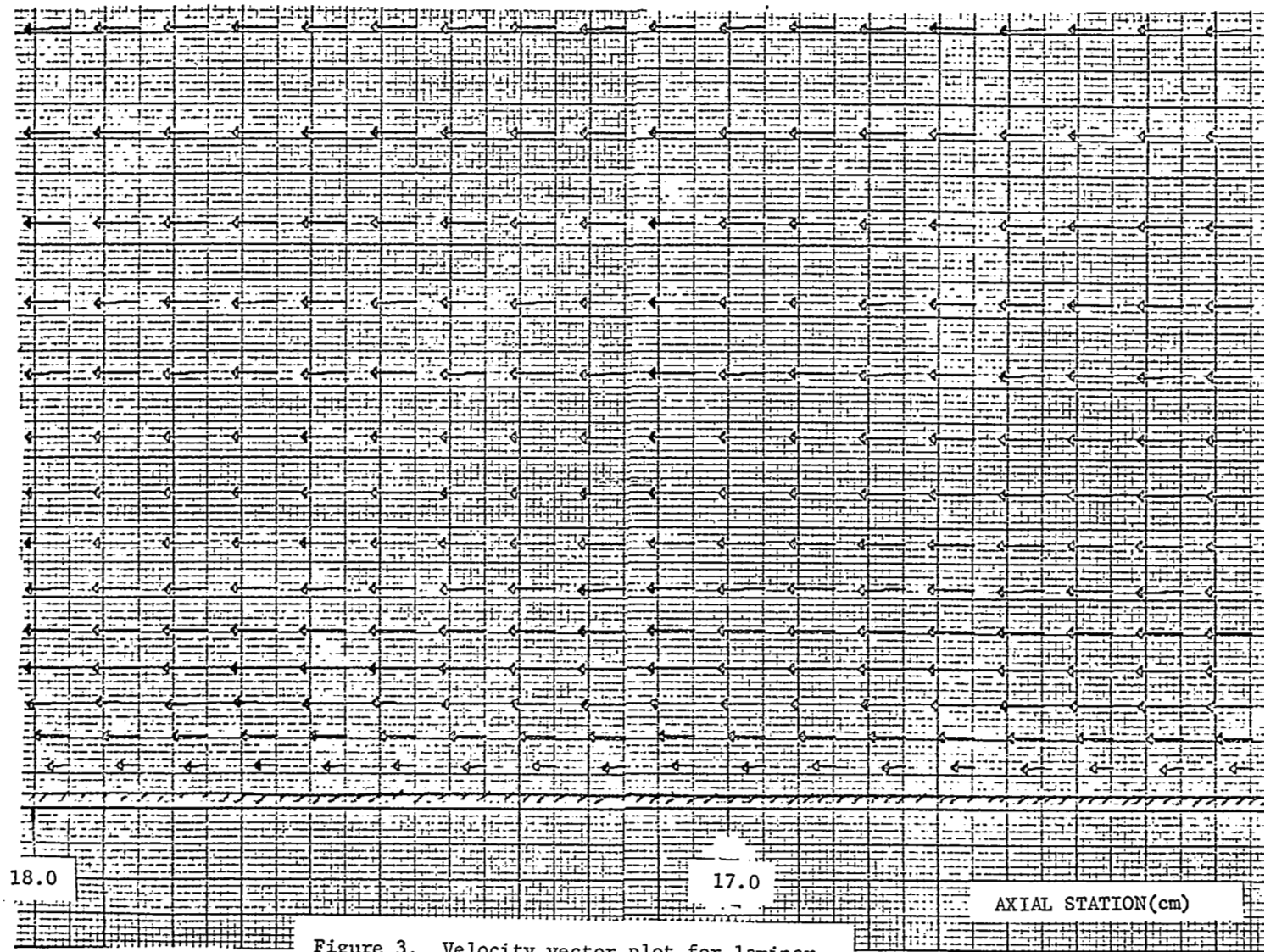

Figure 3. Velocity vector plot for laminar flow over a flat plate at a time when free stream particles have traveled 1.36 plate lengths; Problem 600.0, R = 3.2 x 10^4 per cm; M_∞ = .20.

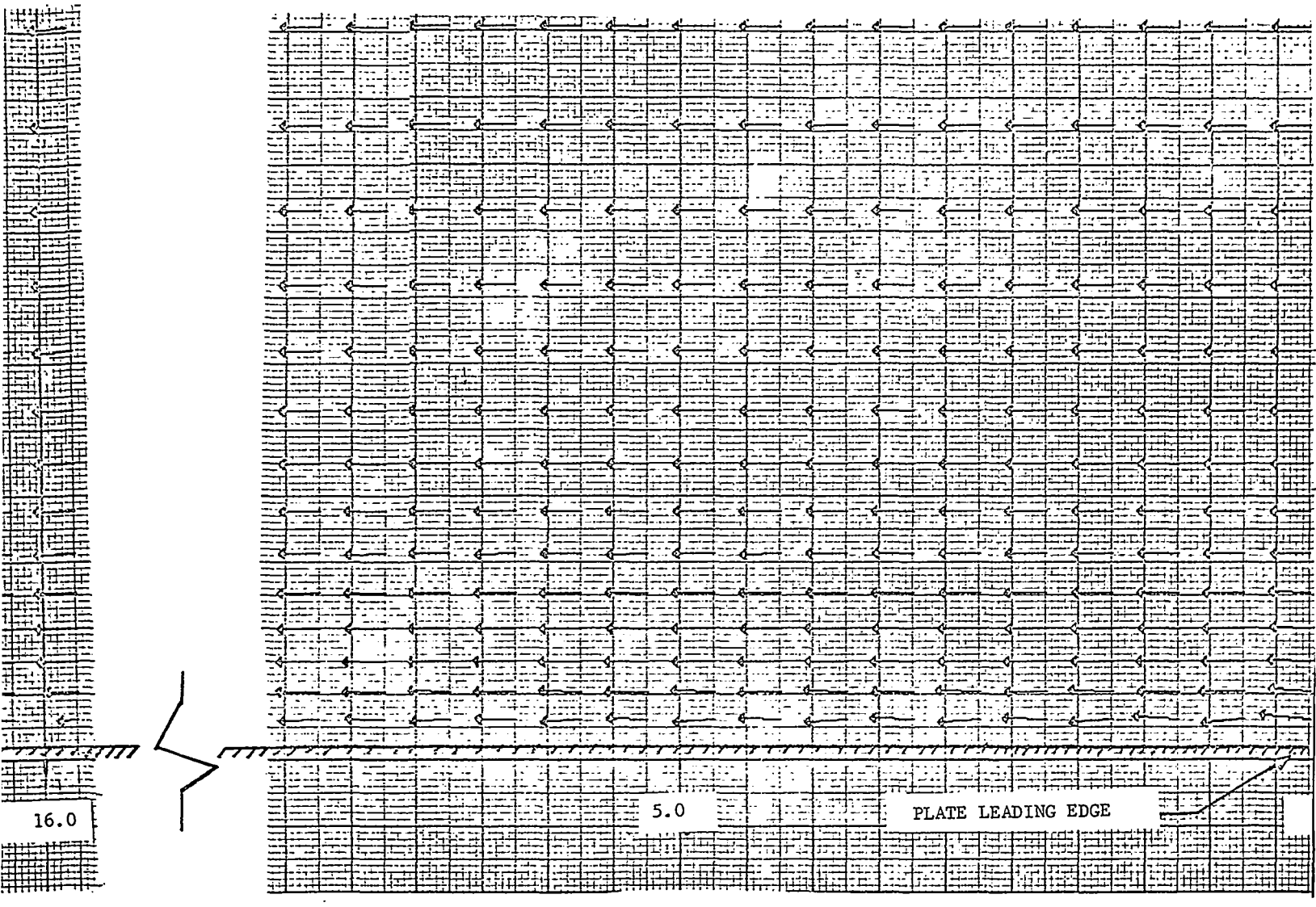
16.0
5.0
PLATE LEADING EDGE

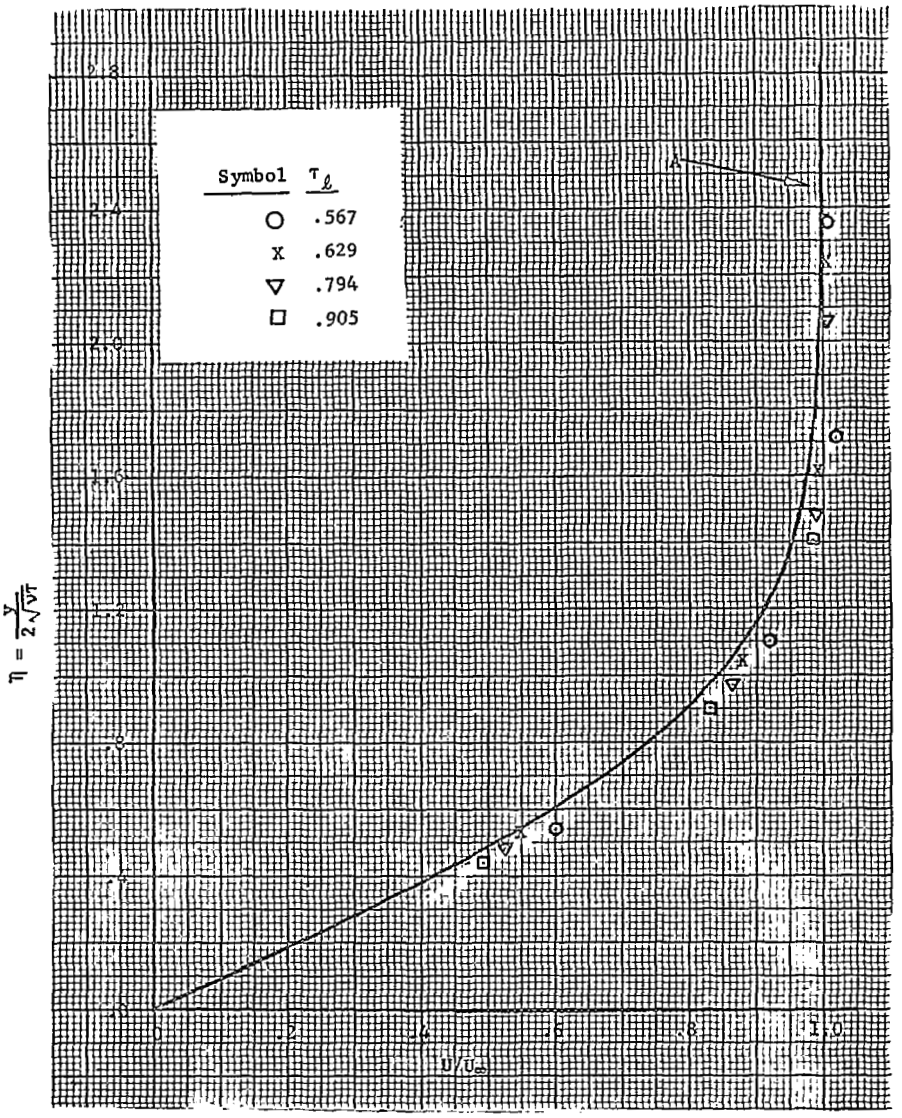

Figure 4. Velocity profile normal to a flat plate under conditions of Rayleigh flow; R = 3.2 x 10^4 per cm, M_∞ = .20; Curve A is the Rayleigh velocity profile; the data points are AFTON 2P output data (Problem 600.0), 12.9 cm aft of the plate leading edge, and at distances normal to the plate of y = .02 cm, y = .041 cm, y = .063 cm, and y = .09 cm; each data symbol represents a time, τ_ℓ, which corresponds to the number of plate lengths of travel by a free stream particle.

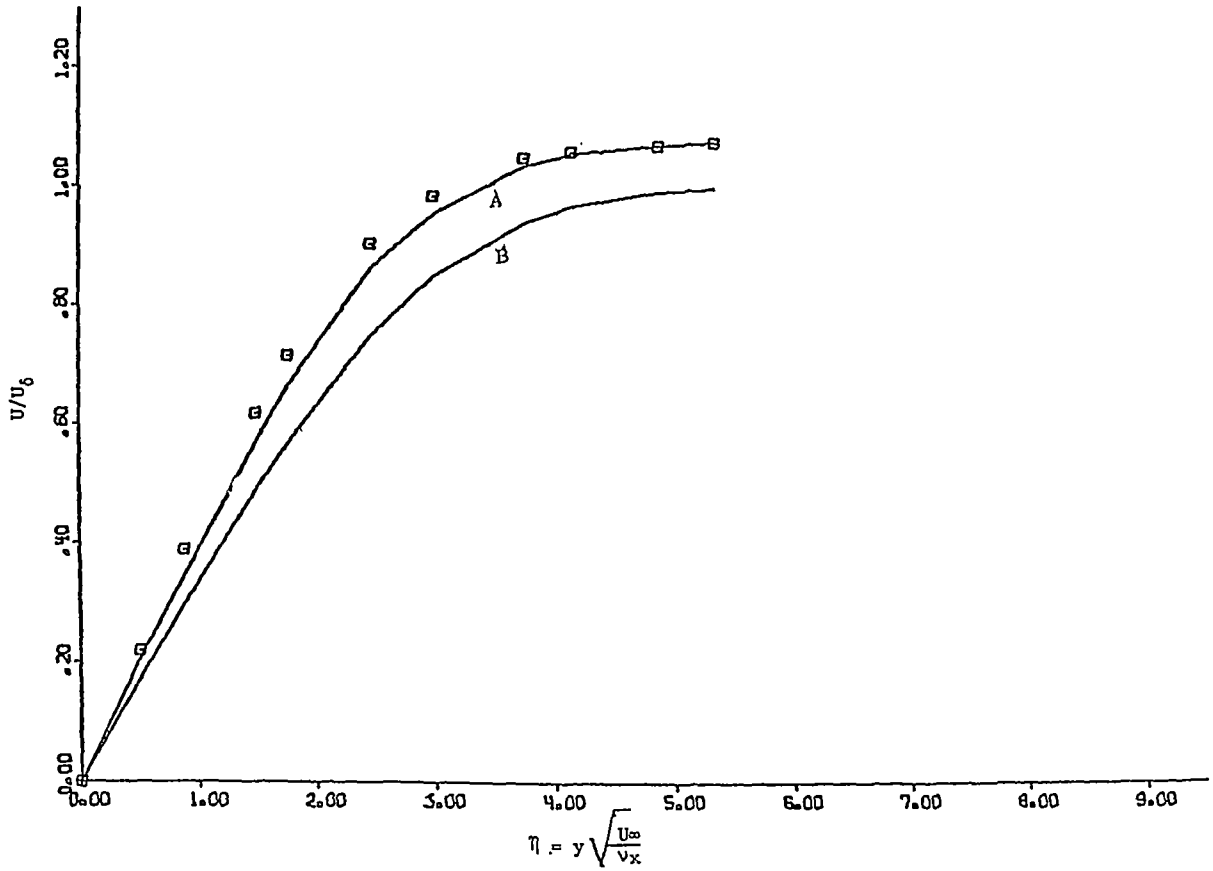

Figure 5. Velocity profile in the boundary layer on a flat plate at Mach 0.20 with a Reynolds number of 3.2×10^4 per cm; Curve A laminar profile in the entrance to a channel, Curve B Blasius flat plate velocity profile, □ AFTON numerical calculations from Problem 600.0.

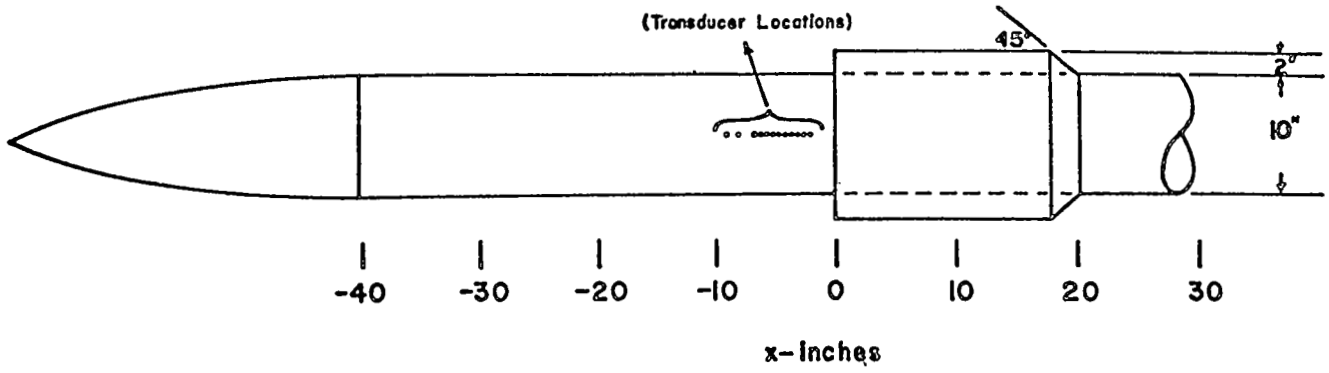

Figure 6. Saturn V wind tunnel configuration experimentally investigated at the Marshall Space Flight Center.

Figure 7. Impulsive initial flow field over a 90^{o} axially symmetric step; numerical data for Problem 2.0 at a Mach number of 1.5 and a Reynolds number per foot of 2.8×10^{6}.

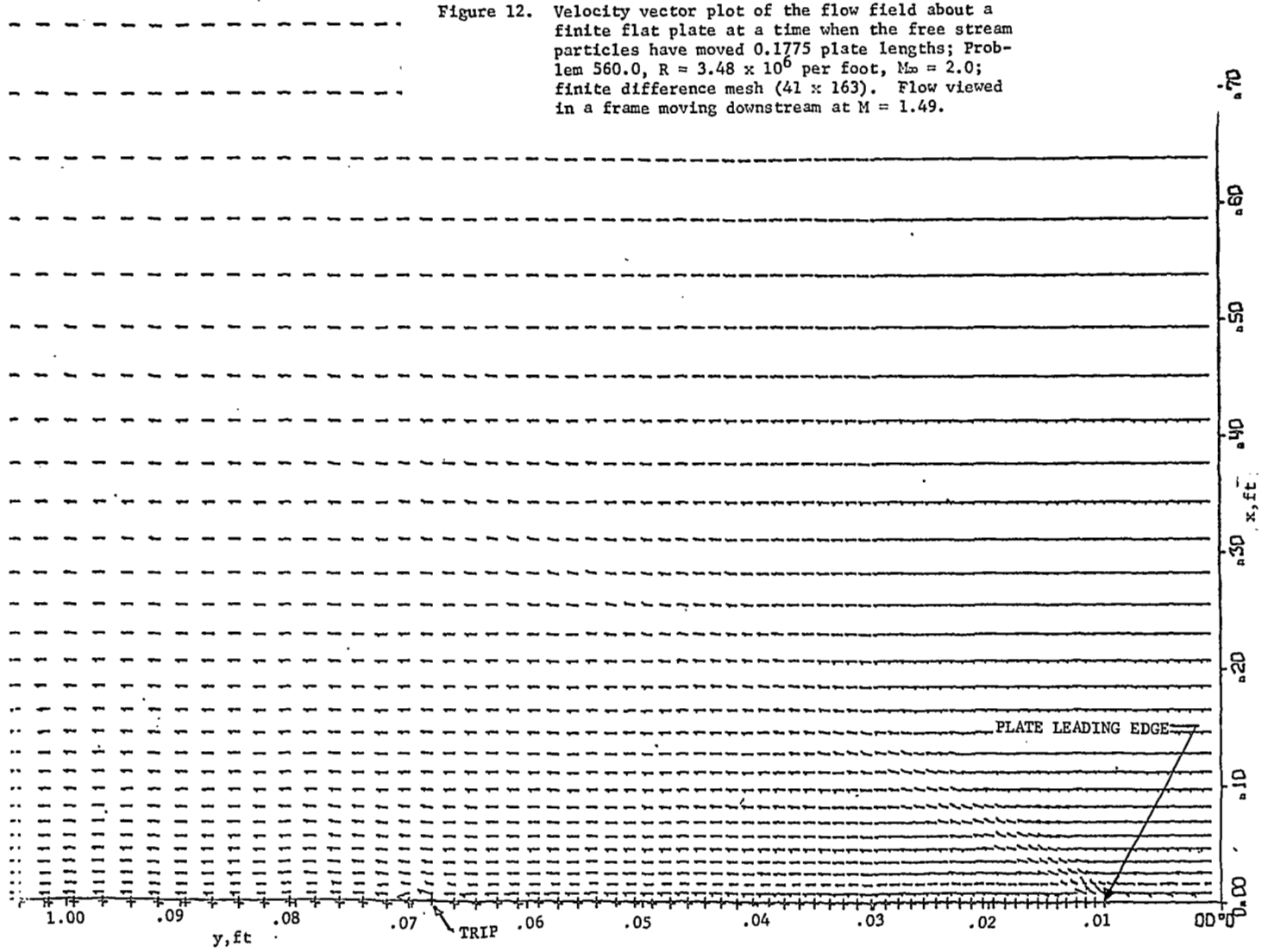

Figure 12. Velocity vector plot of the flow field about a finite flat plate at a time when the free stream particles have moved 0.1775 plate lengths; Problem 560.0, R = 3.48×10^6 per foot, $M_\infty = 2.0$; finite difference mesh (41 x 163). Flow viewed in a frame moving downstream at M = 1.49.

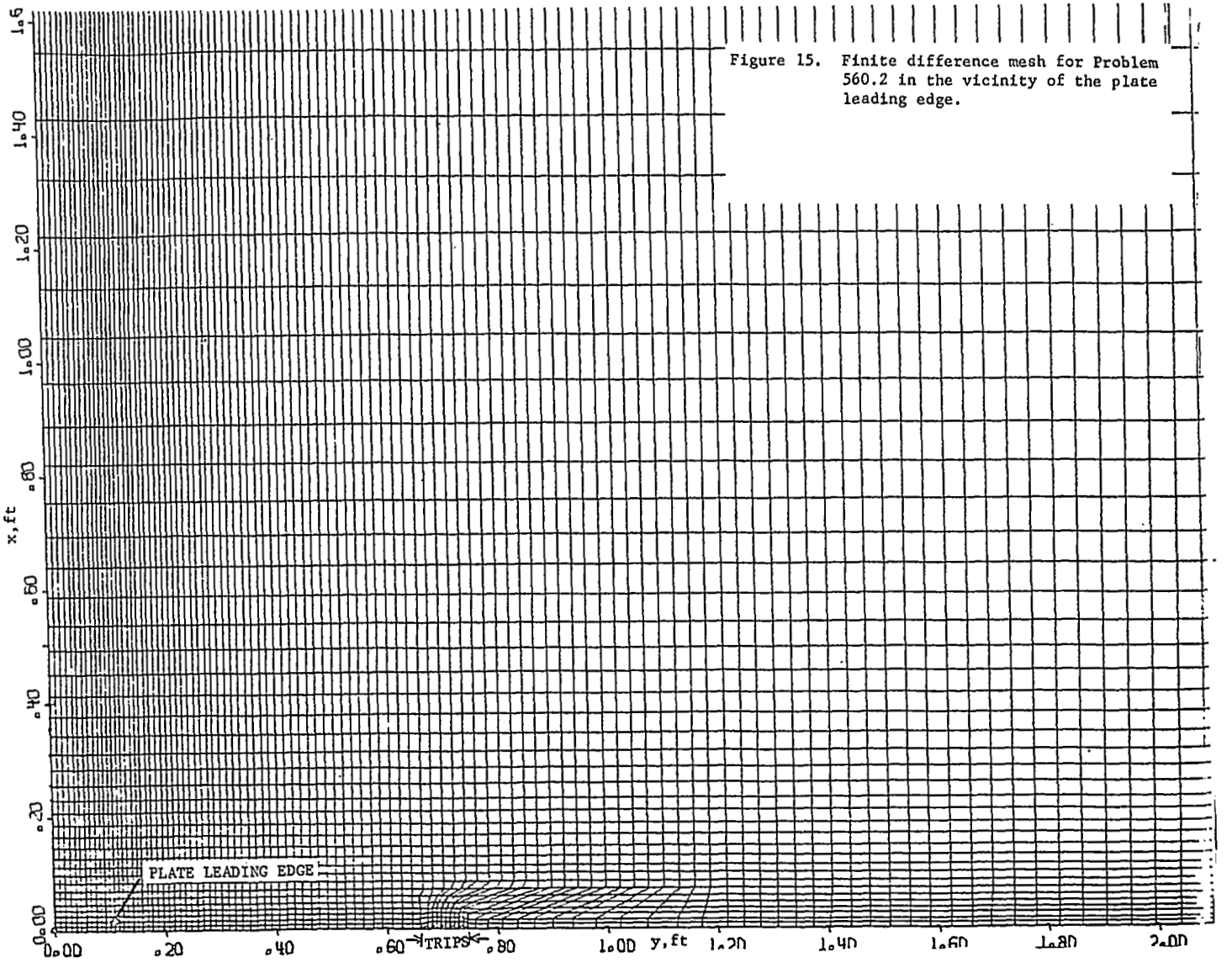

Figure 15. Finite difference mesh for Problem 560.2 in the vicinity of the plate leading edge.

Figure 12. Velocity vector plot of the flow field about a finite flat plate at a time when the free stream particles have moved 0.1775 plate lengths; Problem 560.0, R = 3.48×10^6 per foot, $M_\infty = 2.0$; finite difference mesh (41 x 163). Flow viewed in a frame moving downstream at M = 1.49.

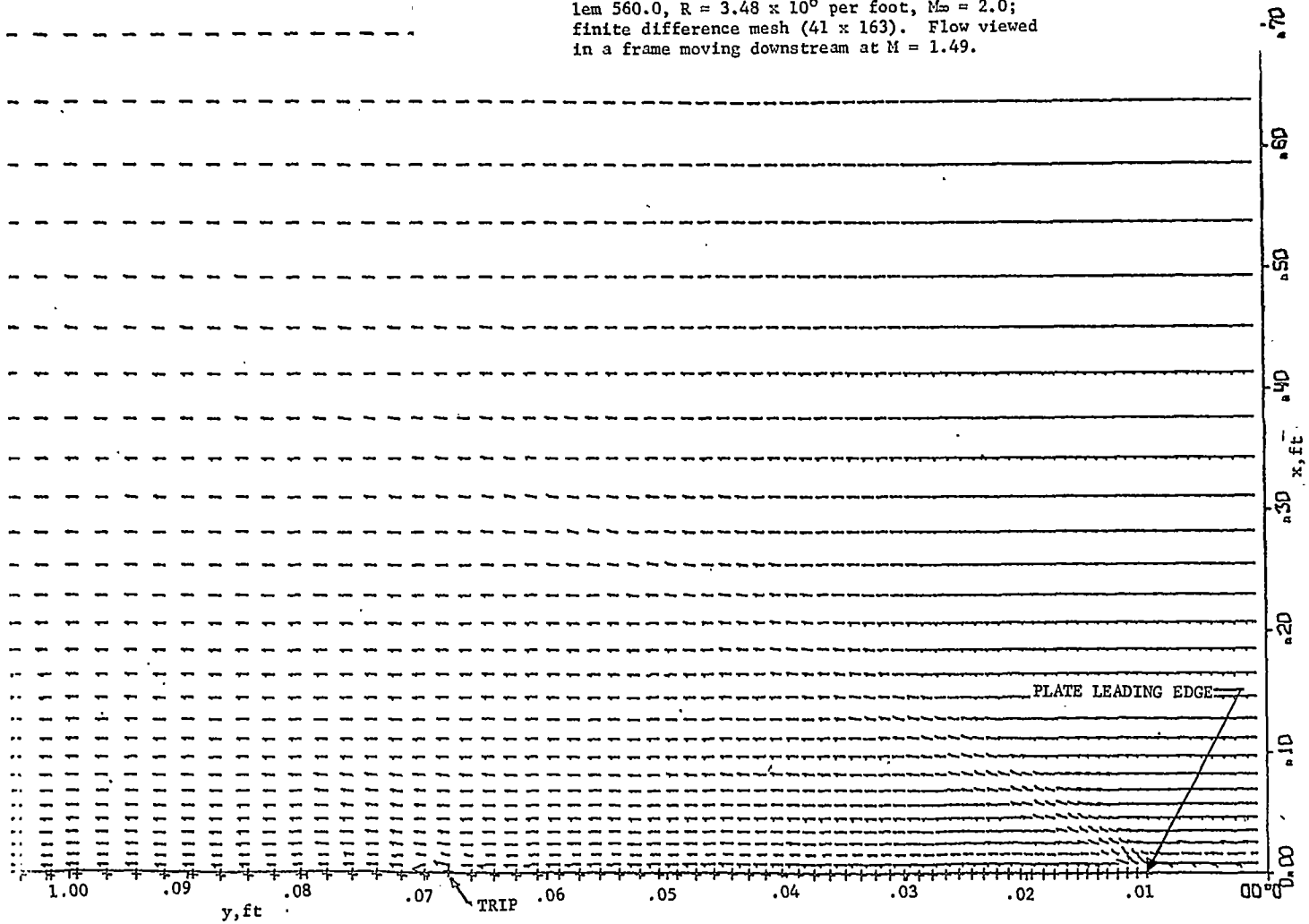

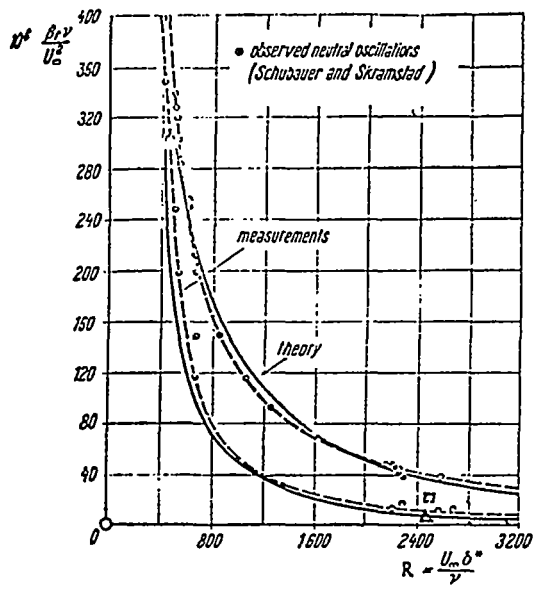

Figure 13. Curves of neutral stability for neutral frequencies of disturbances on a flat plate at zero incidence.[18] The point Δ corresponds to the flow field conditions of the numerical calculation for a single trip; $\square$ refers to the numerical calculation with five trips.

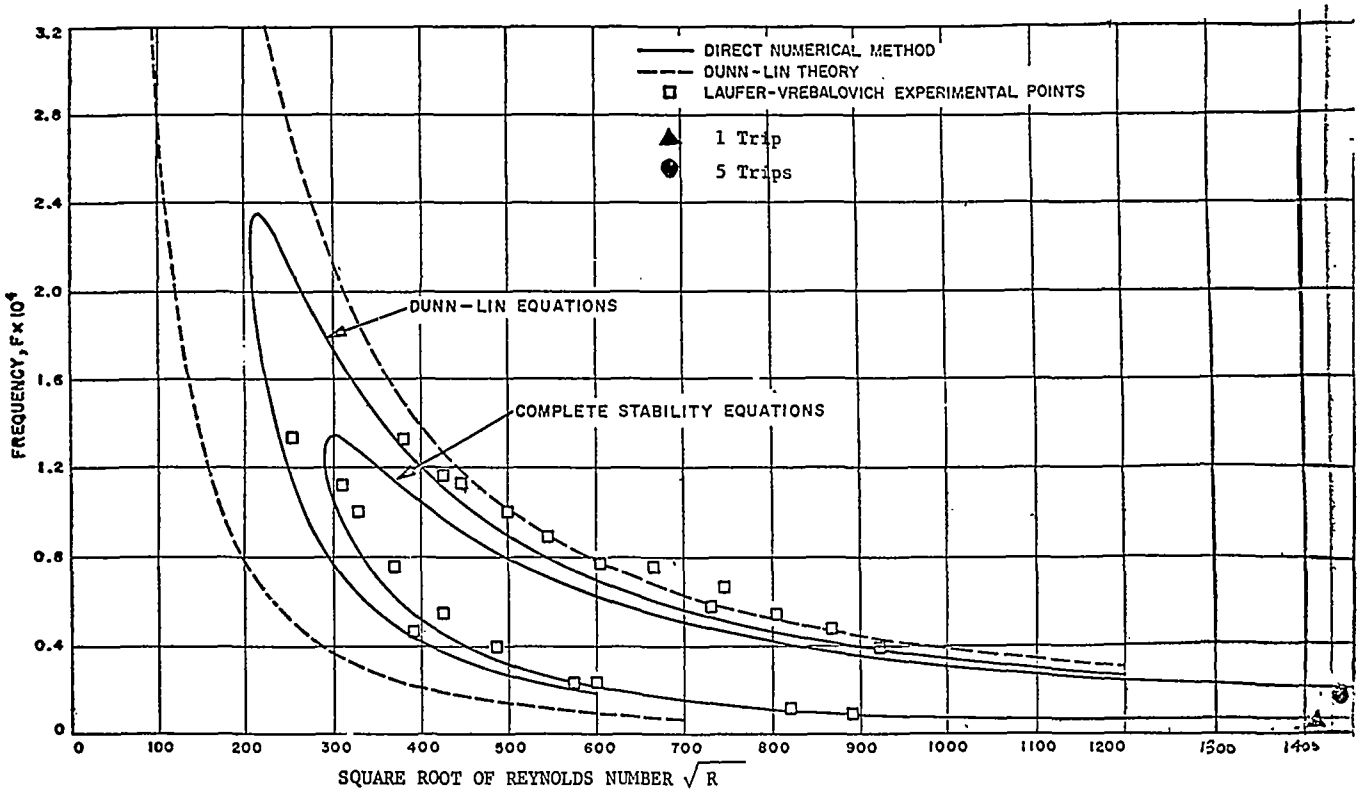

Figure 14. Neutral-stability curves of frequency versus Reynolds number at $M_\infty = 2.2$ for insulated-wall boundary layer.[19]

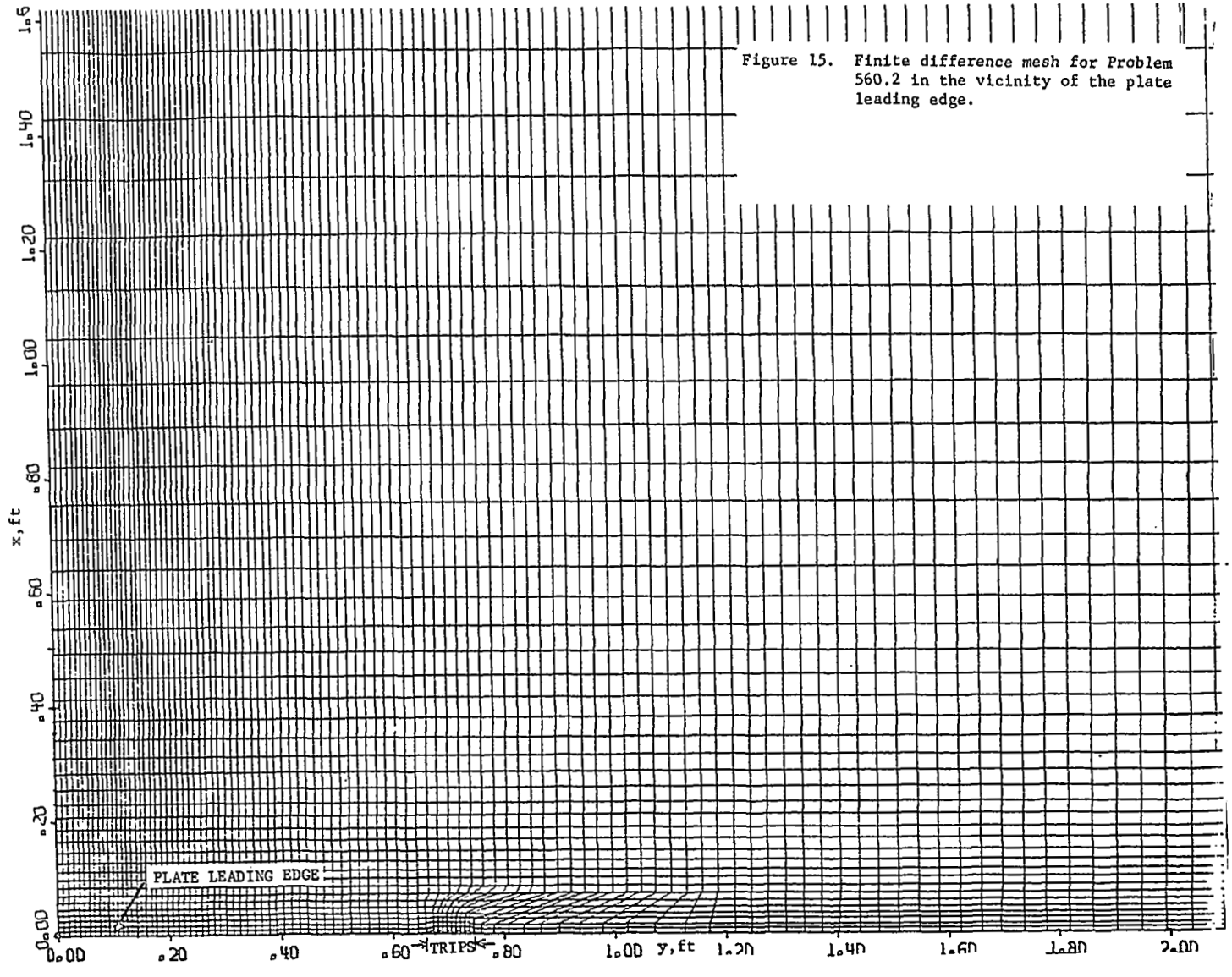

Figure 15. Finite difference mesh for Problem 560.2 in the vicinity of the plate leading edge.

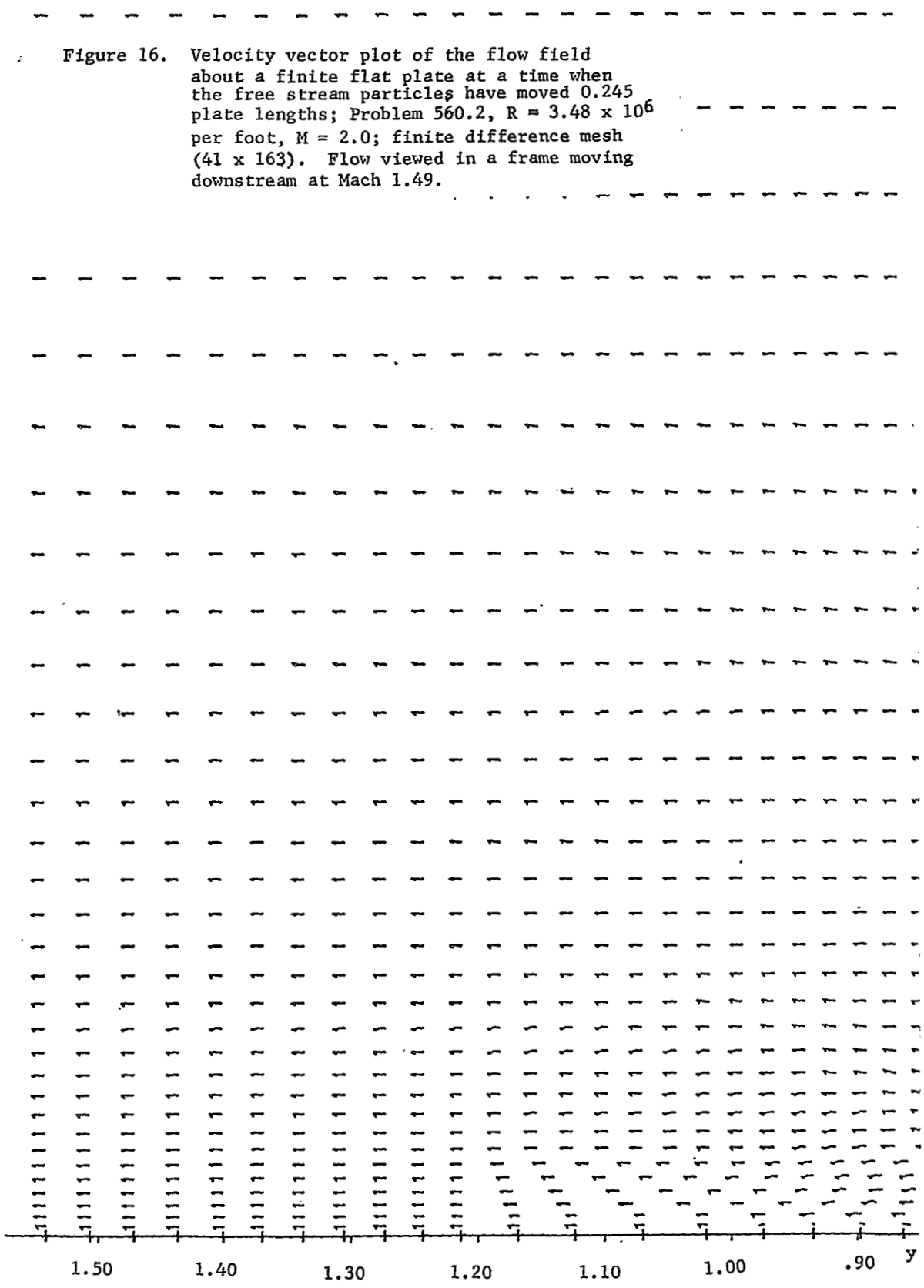

Figure 16. Velocity vector plot of the flow field about a finite flat plate at a time when the free stream particles have moved 0.245 plate lengths; Problem 560.2, R = 3.48 x 10^6 per foot, M = 2.0; finite difference mesh (41 x 163). Flow viewed in a frame moving downstream at Mach 1.49.

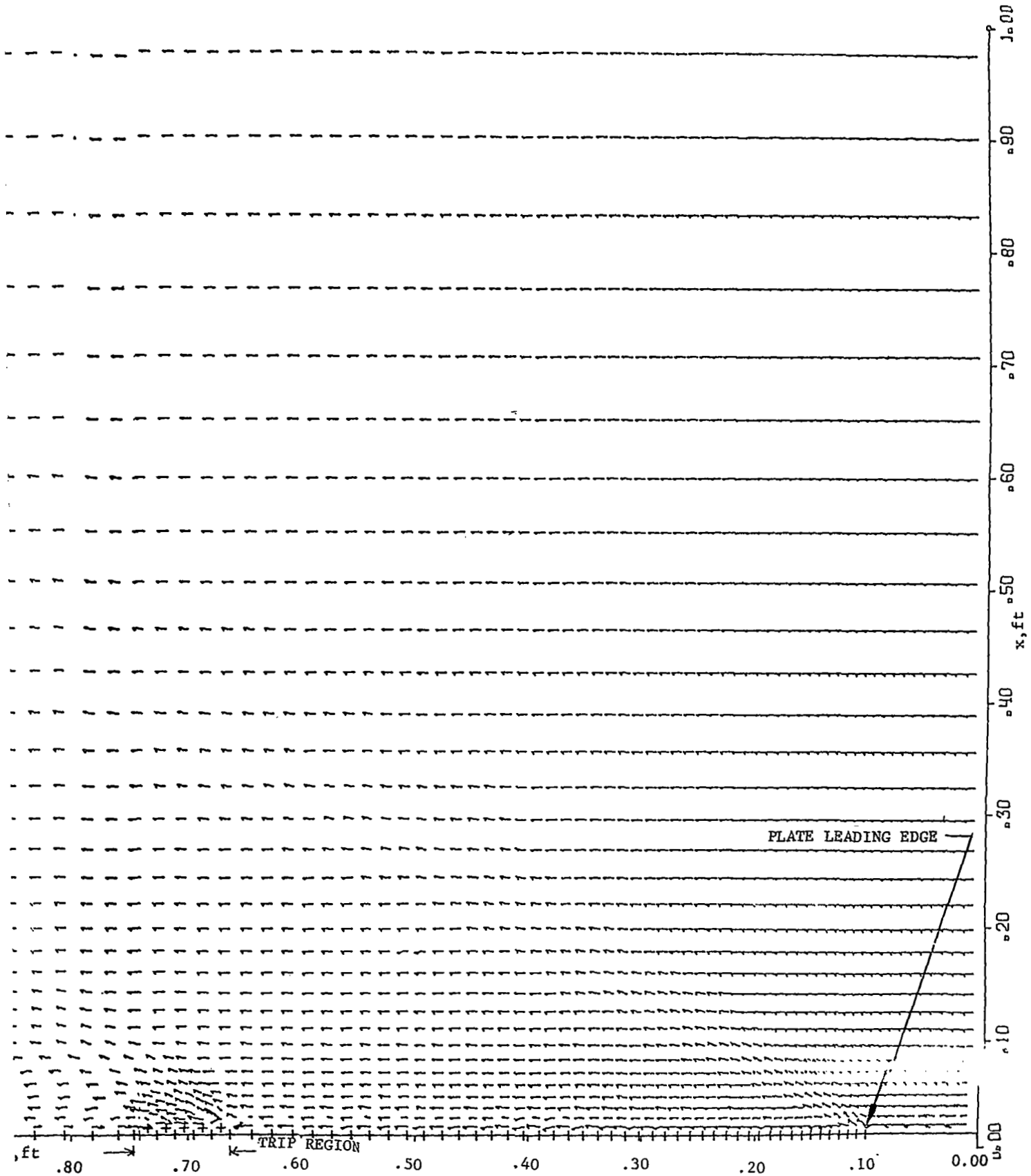
PLATE LEADING EDGE
TRIP REGION
x,ft
1.00
.90
.80
.70
.60
.50
.40
.30
.20
.10
0.00
,ft
.80
.70
.60
.50
.40
.30
.20
.10
0.00

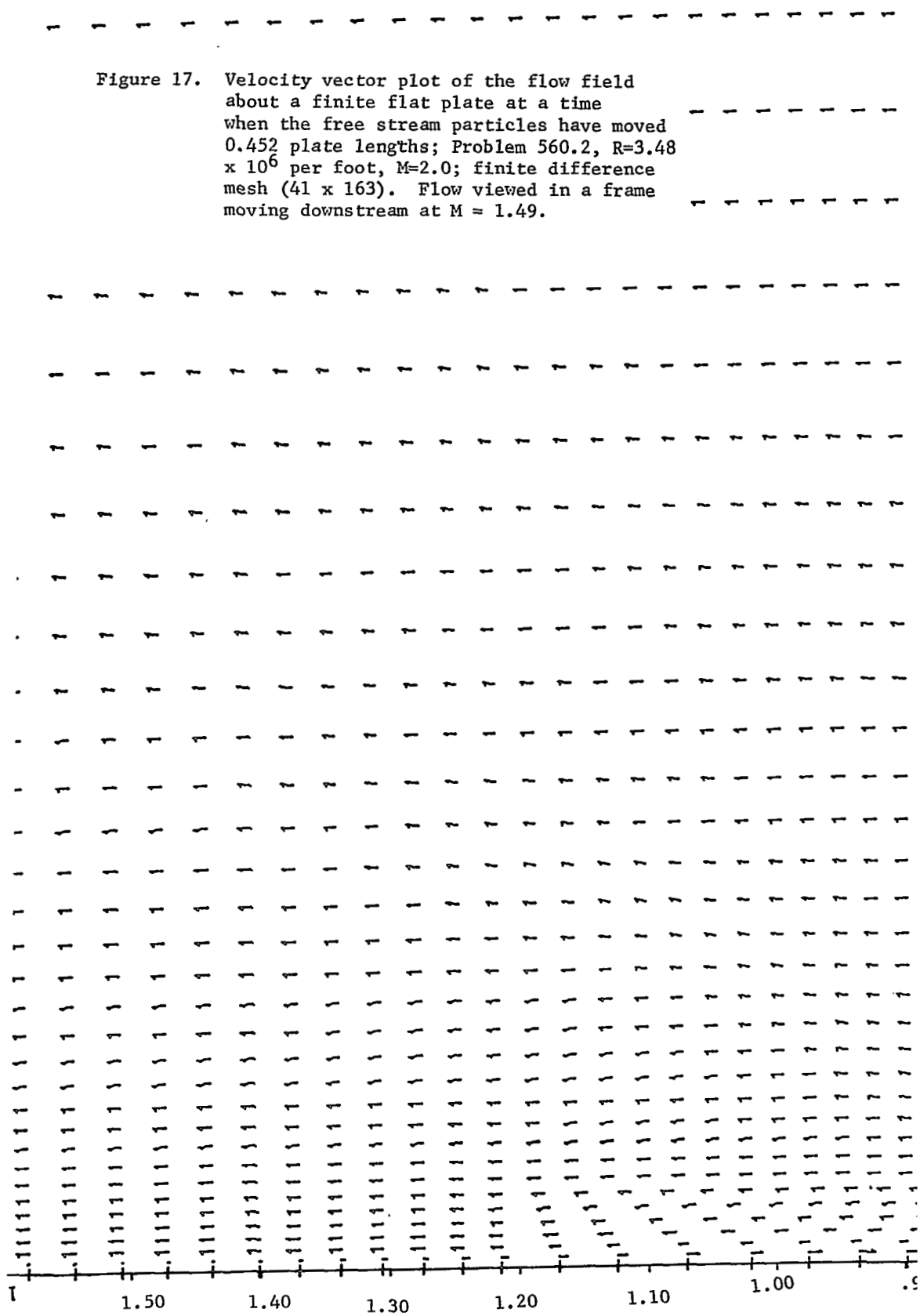

Figure 17. Velocity vector plot of the flow field about a finite flat plate at a time when the free stream particles have moved 0.452 plate lengths; Problem 560.2, R=3.48 x 10^6 per foot, M=2.0; finite difference mesh (41 x 163). Flow viewed in a frame moving downstream at M = 1.49.

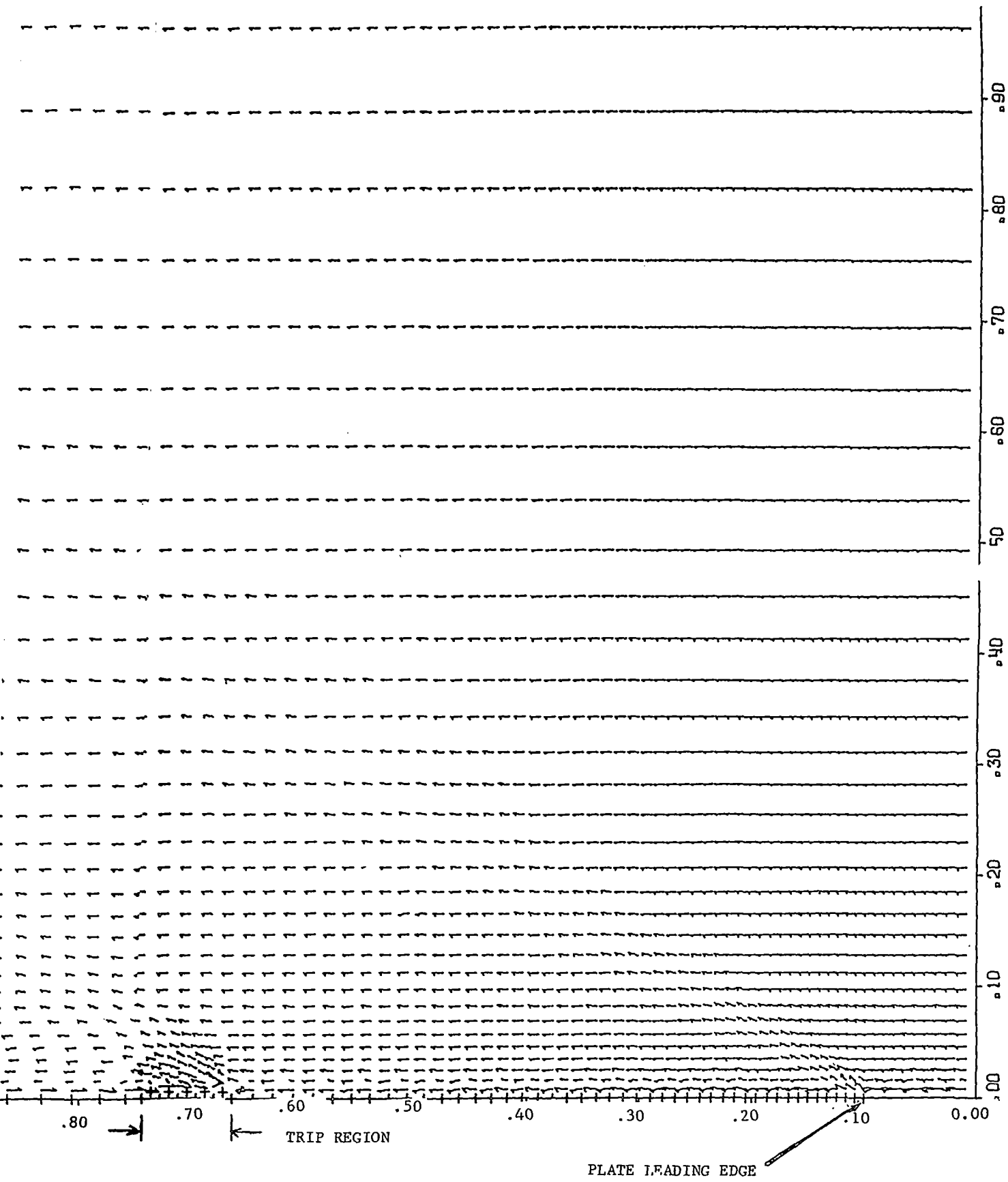
.90
.80
.70
.60
.50
.40
.30
.20
.10
.00
.80
.70
.60
.50
.40
.30
.20
.10
0.00
TRIP REGION
PLATE LEADING EDGE

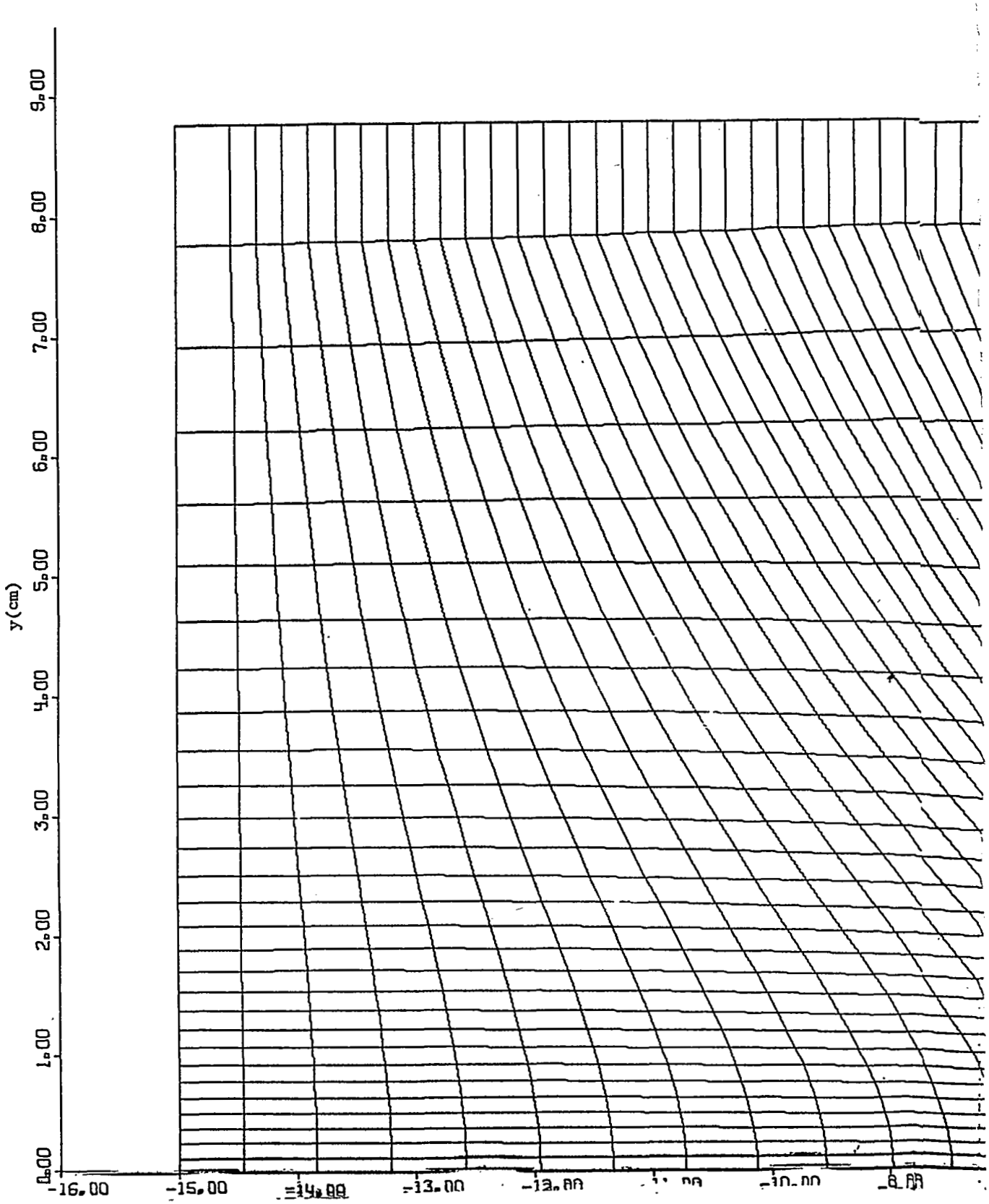
y(cm)
9.00
8.00
7.00
6.00
5.00
4.00
3.00
2.00
1.00
0.00
-16.00
-15.00
-14.00
-13.00
-12.00
-10.00

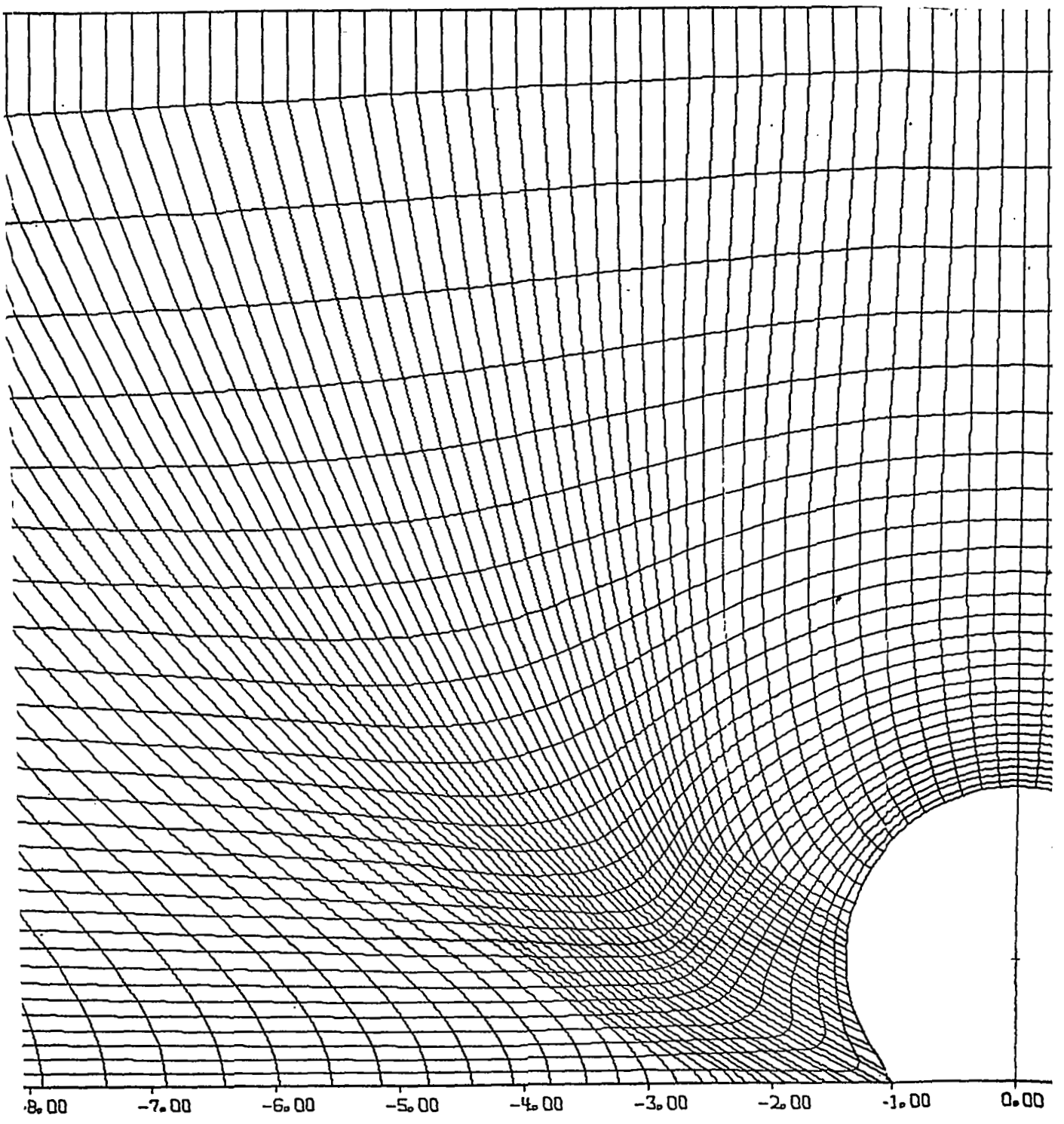
-8.00
-7.00
-6.00
-5.00
-4.00
-3.00
-2.00
-1.00
0.00

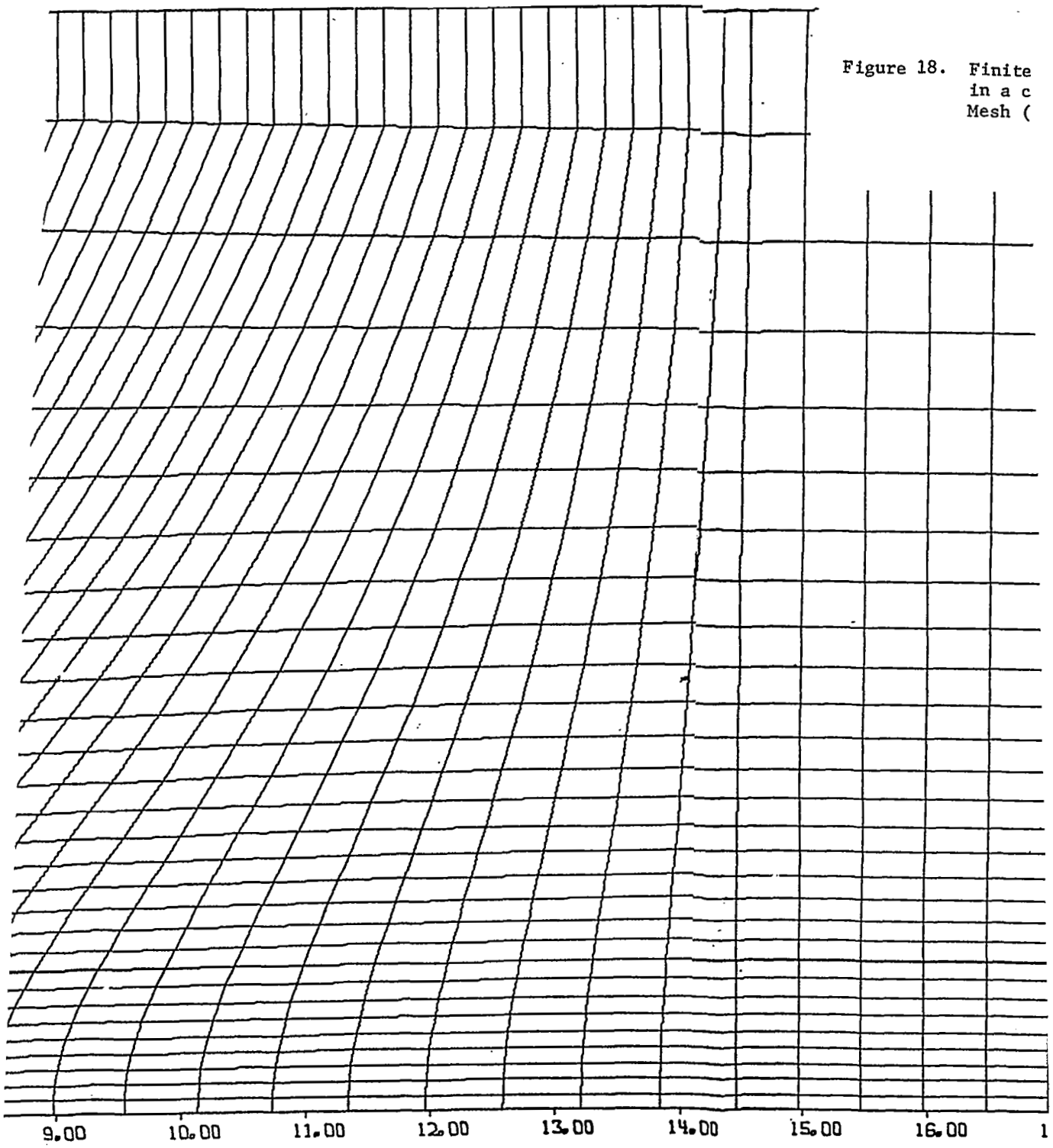

Figure 18. Finite
in a c
Mesh (

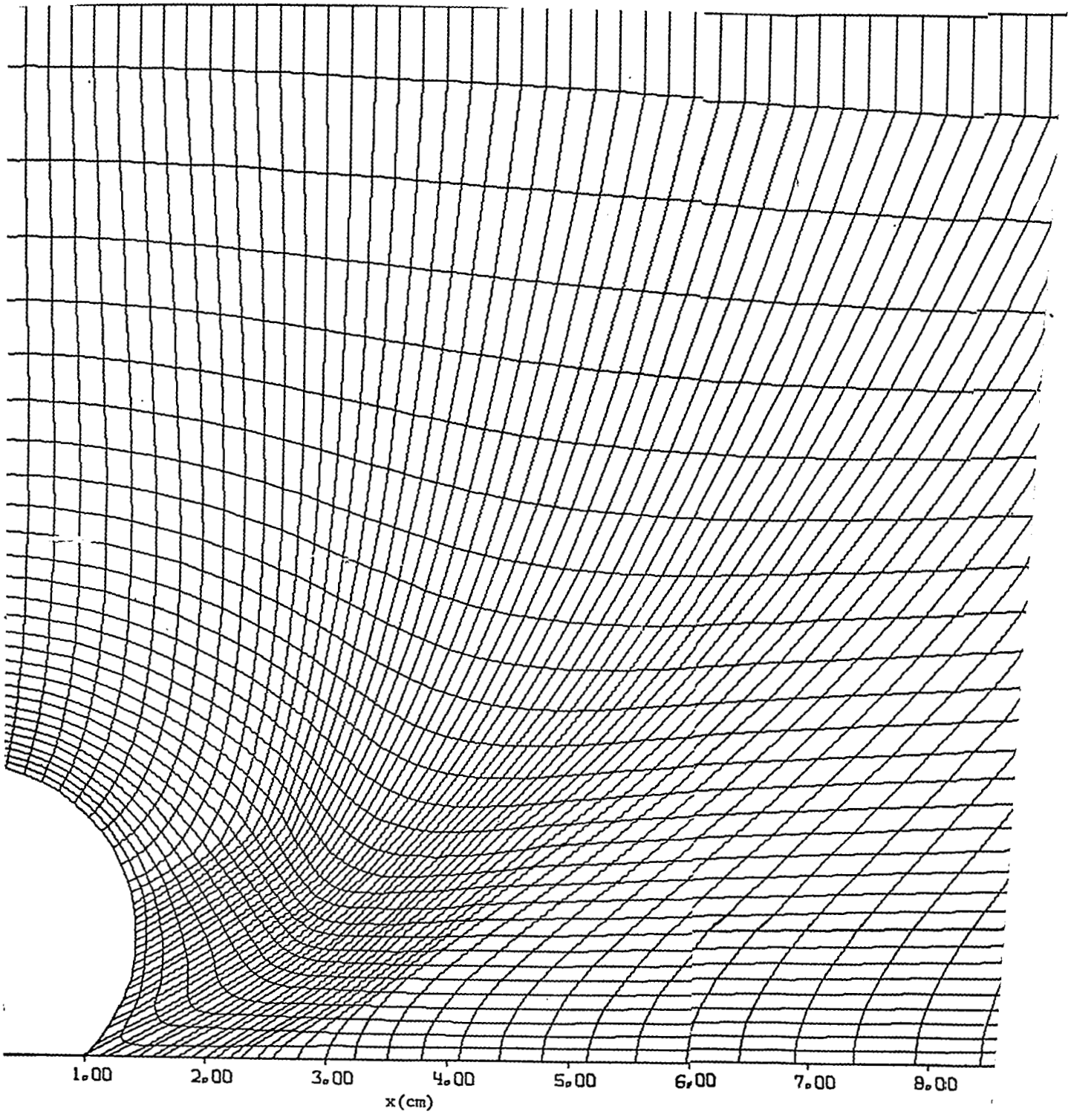
1.00
2.00
3.00
4.00
5.00
6.00
7.00
8.00
x(cm)

Figure 18. Finite difference mesh for flow in a channel with a wire trip; Mesh (30 x 157); Problem 561.0.

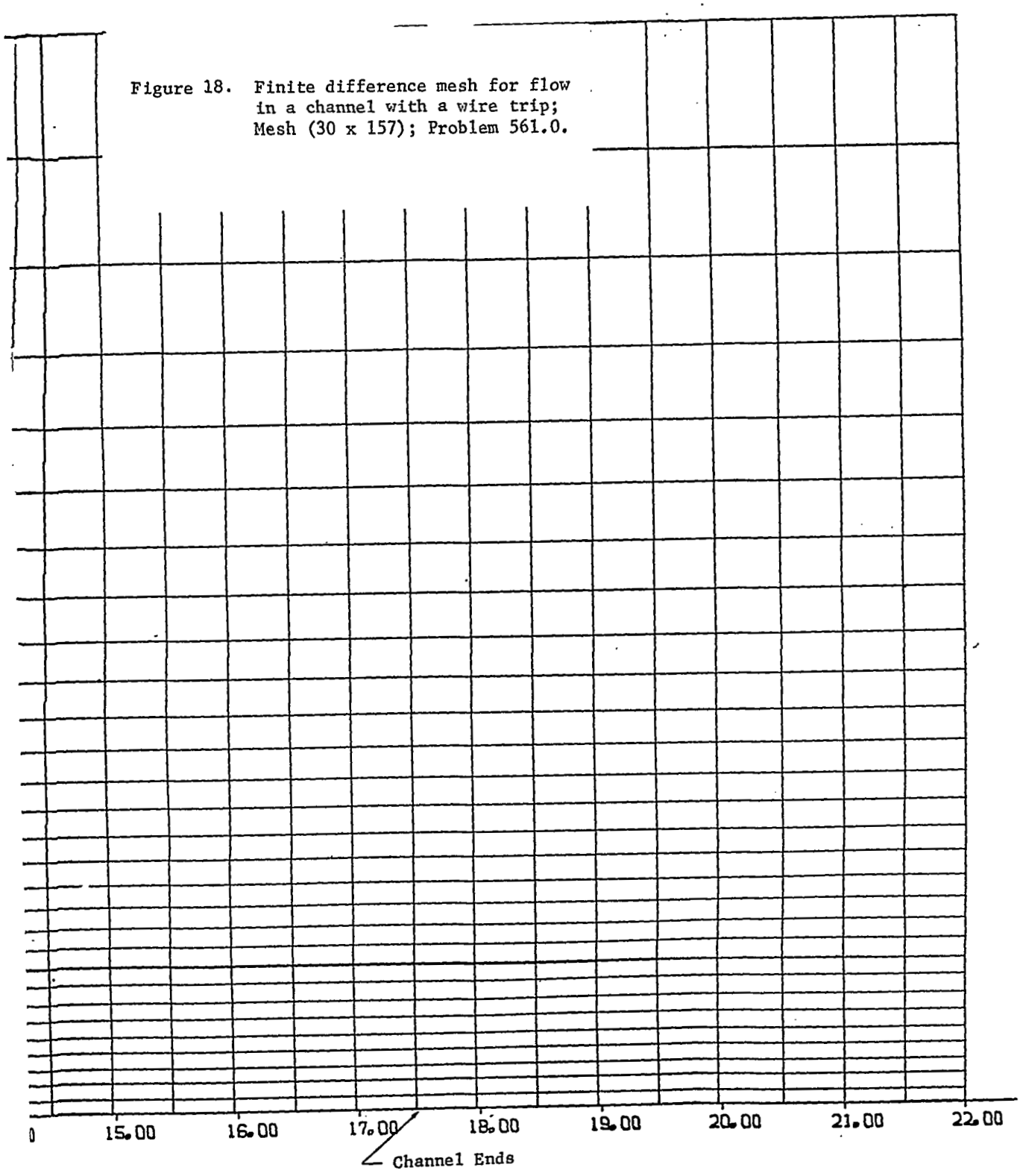

Figure 19. Velocity vector plot of the flow field about a wire trip in a channel at a time when the particles along the channel centerline have moved 0.0 trip heights; Problem 561.0, R_D(Avg.) = 10000.0, M(Avg.) = .20; finite difference mesh (30 x 157).

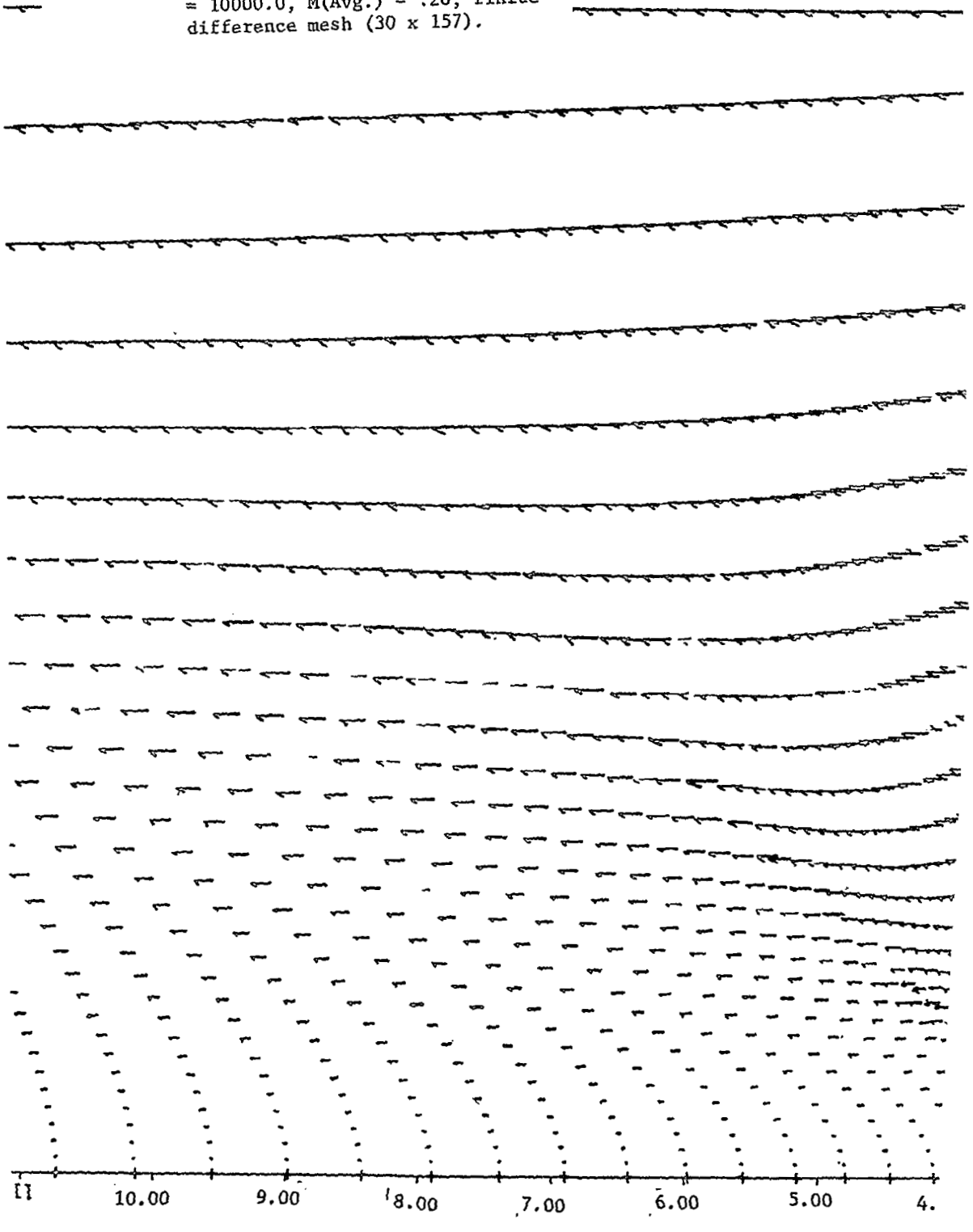

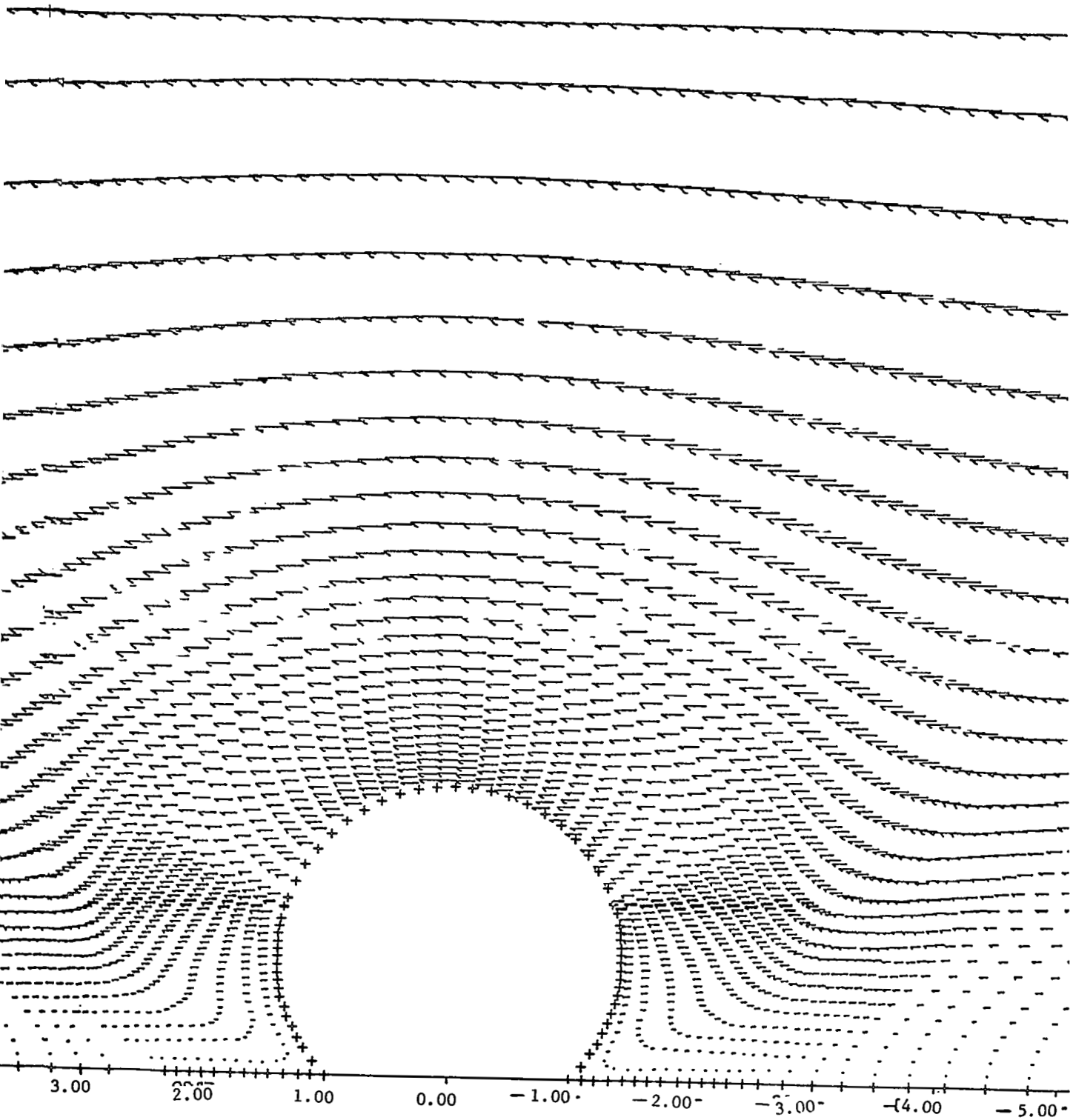
3.00
2.00
1.00
0.00
-1.00
-2.00
-3.00
-4.00
-5.00

Figure 20. Velocity vector plot of the flow field about a wire trip in a channel at a time when the particles along the channel centerline have moved 1.4 trip heights; Problem 561.0, R_D(Avg.) = 10000.0, M(Avg.) = .20; finite difference mesh (30 x 157).

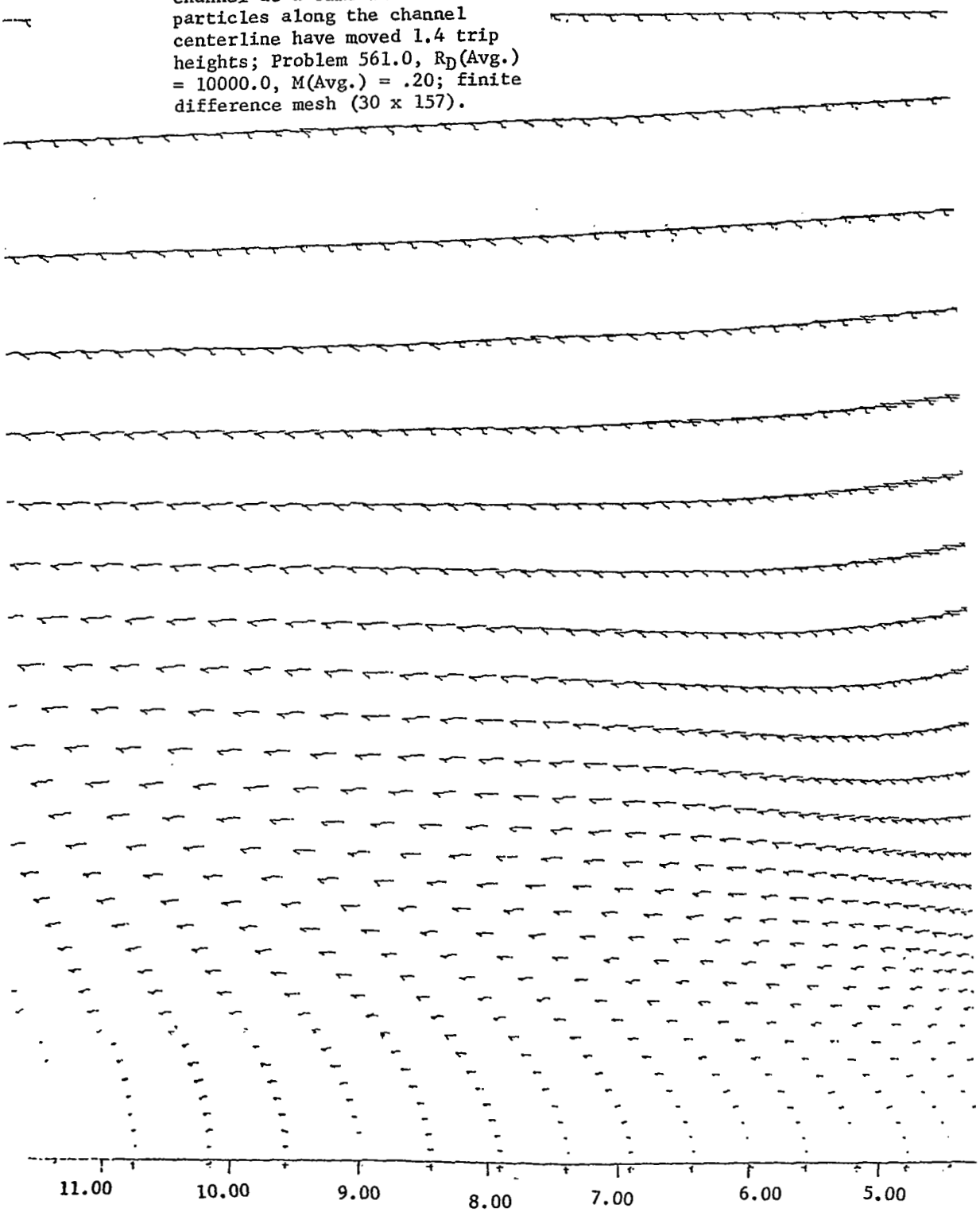

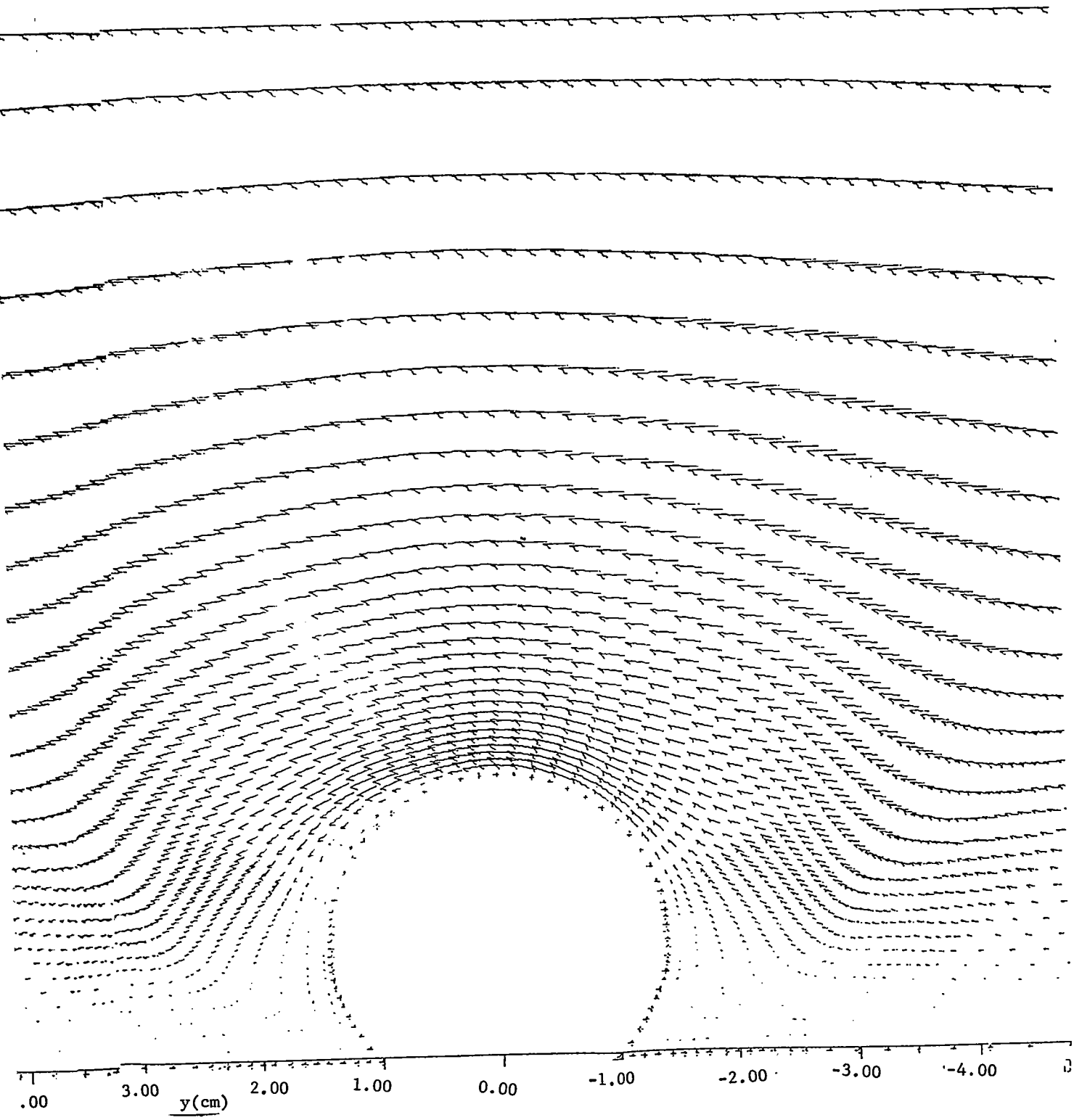
.00
3.00
y(cm)
2.00
1.00
0.00
-1.00
-2.00
-3.00
-4.00

Figure 21. Velocity vector plot of the flow field about a wire trip in a channel at a time when the particles along the channel centerline have moved 2.95 trip heights; Problem 561.0, R_D(Avg.) = 10000.0, M(Avg.) = .20; finite difference mesh (30 x 157).

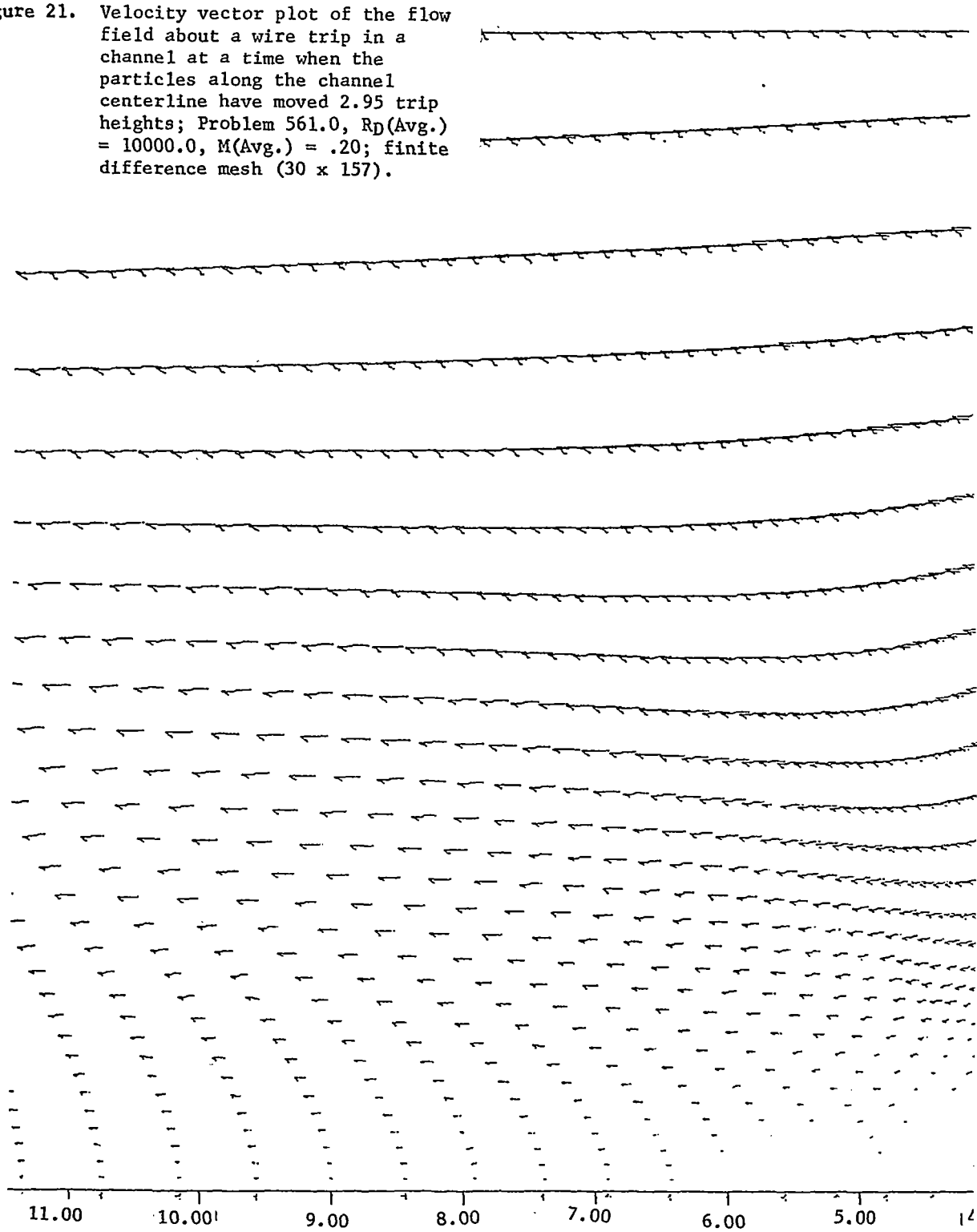

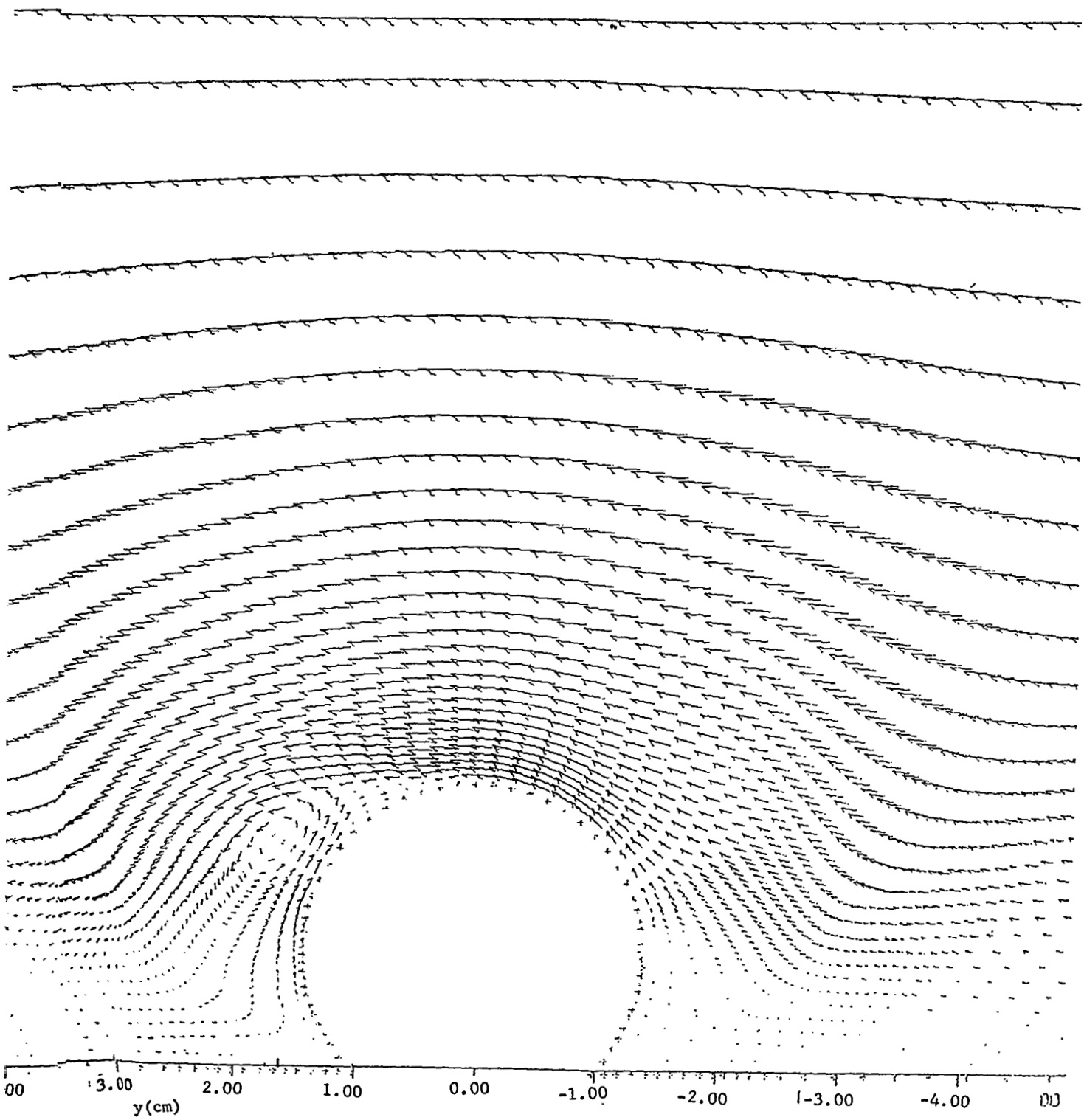
00
3.00
2.00
1.00
0.00
-1.00
-2.00
-3.00
-4.00
00
y(cm)

Figure 22. Velocity vector plot of the flow field about a wire trip in a channel at a time when the particles along the channel centerline have moved 5.75 trip heights; Problem 561.0, R_D(Avg.) = 1000.0, M(Avg.) = .20; finite difference mesh (30 x 157).

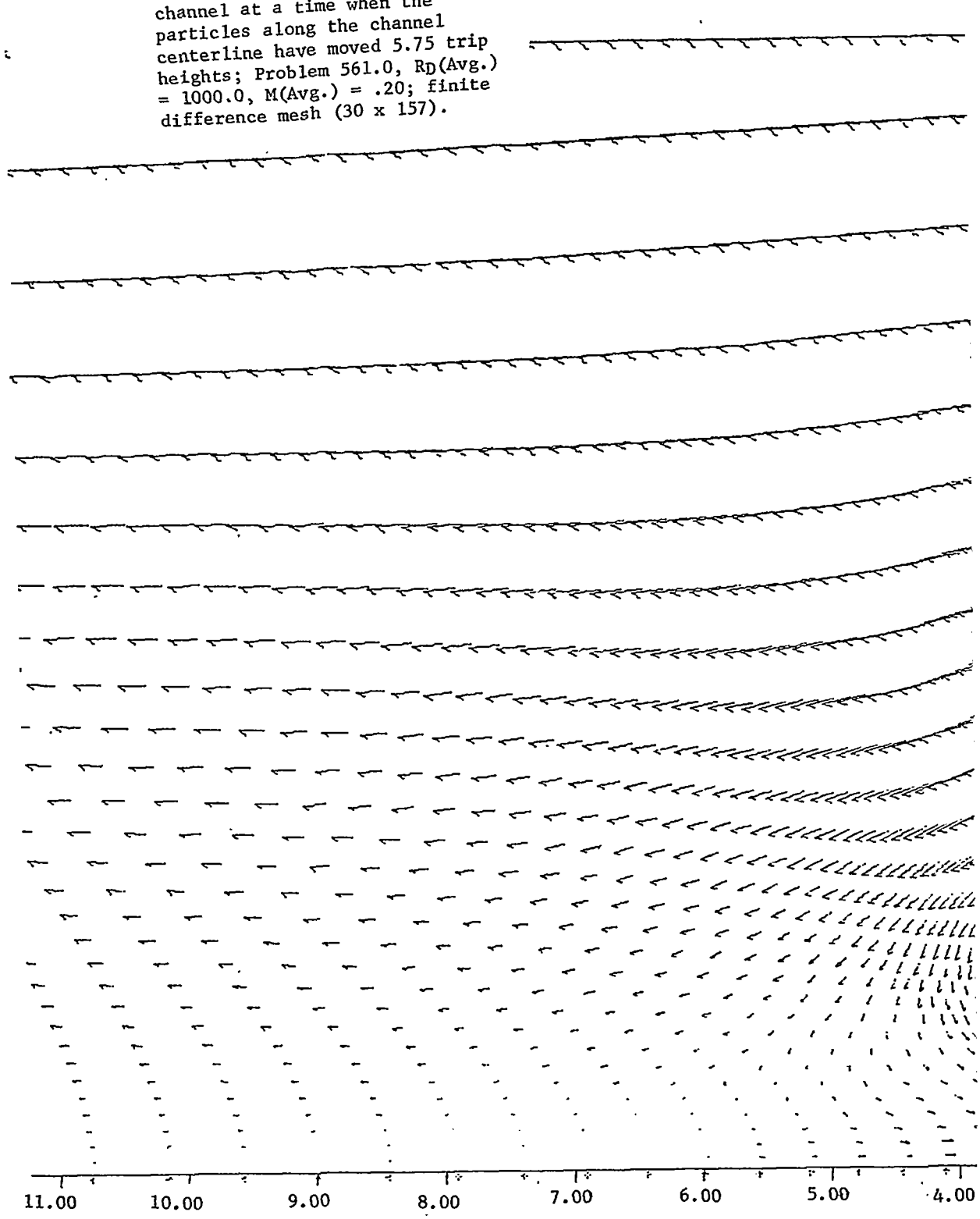

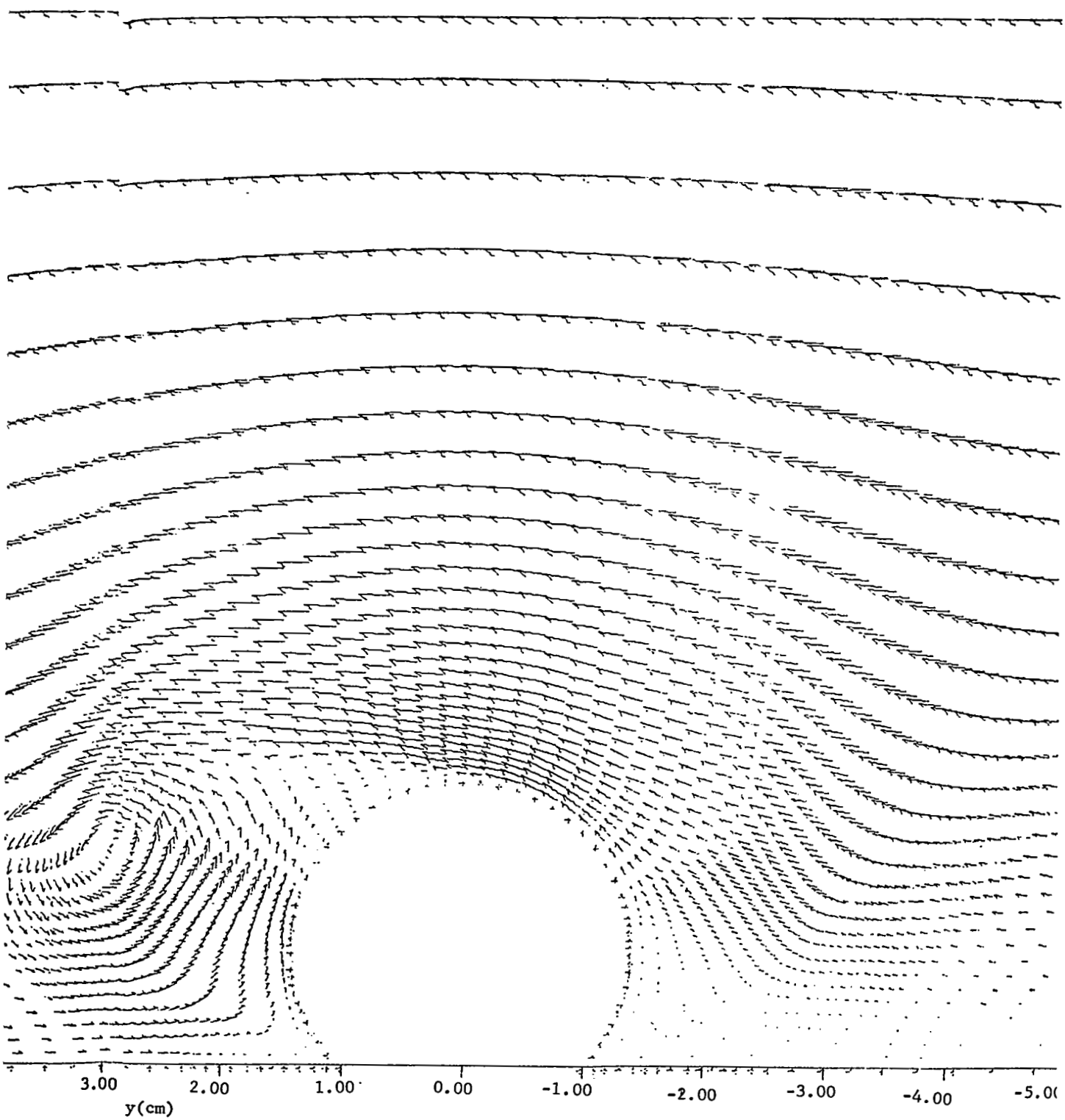
3.00
2.00
1.00
0.00
-1.00
-2.00
-3.00
-4.00
-5.0(
y(cm)

Figure 23. Velocity vector plot of the flow field about a wire trip in a channel at a time when the particles along the channel centerline have moved 8.35 trip heights; Problem 561.0, R_D(Avg.) = 10000.0, M(Avg.) = .20; finite difference mesh (30 x 157).

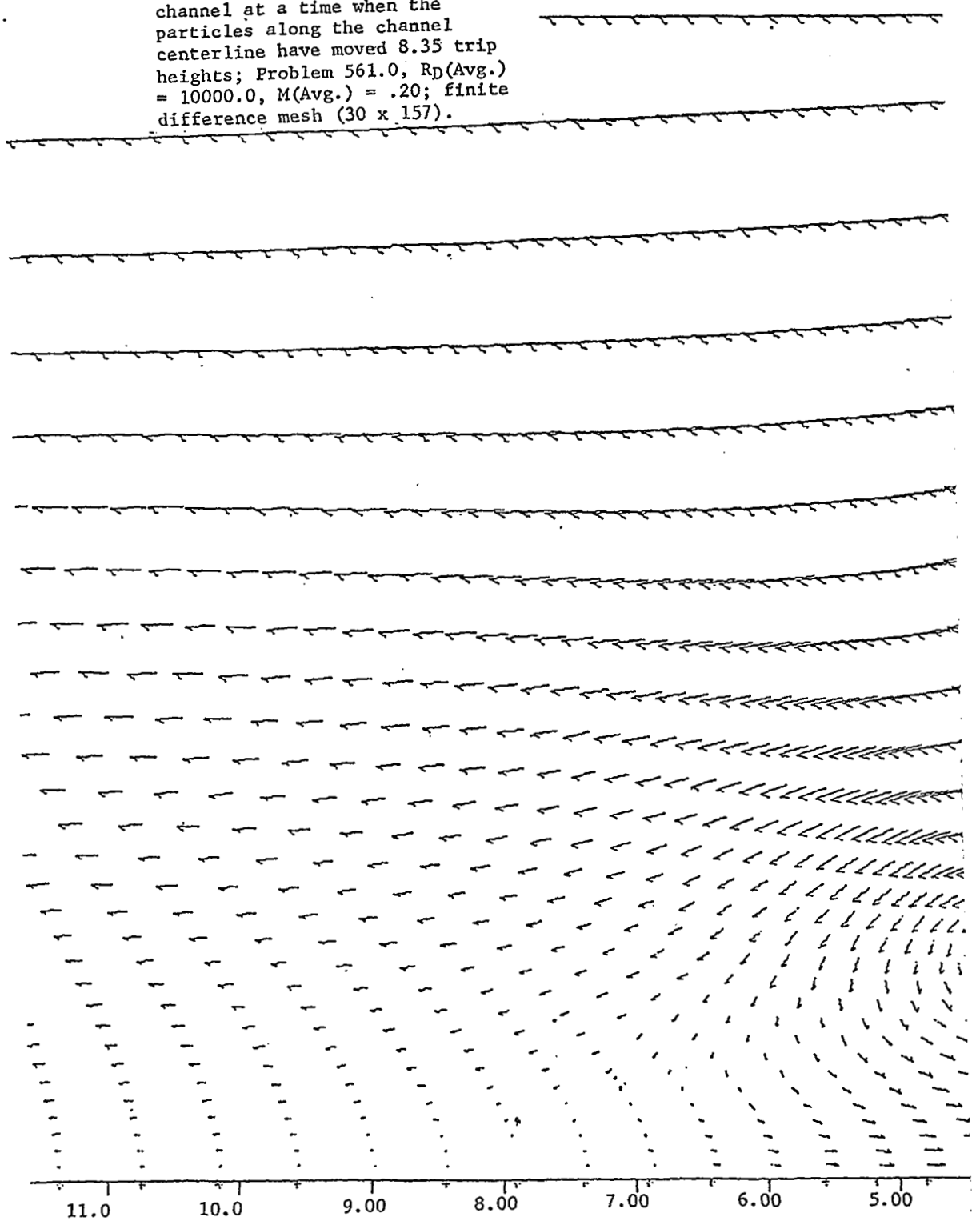

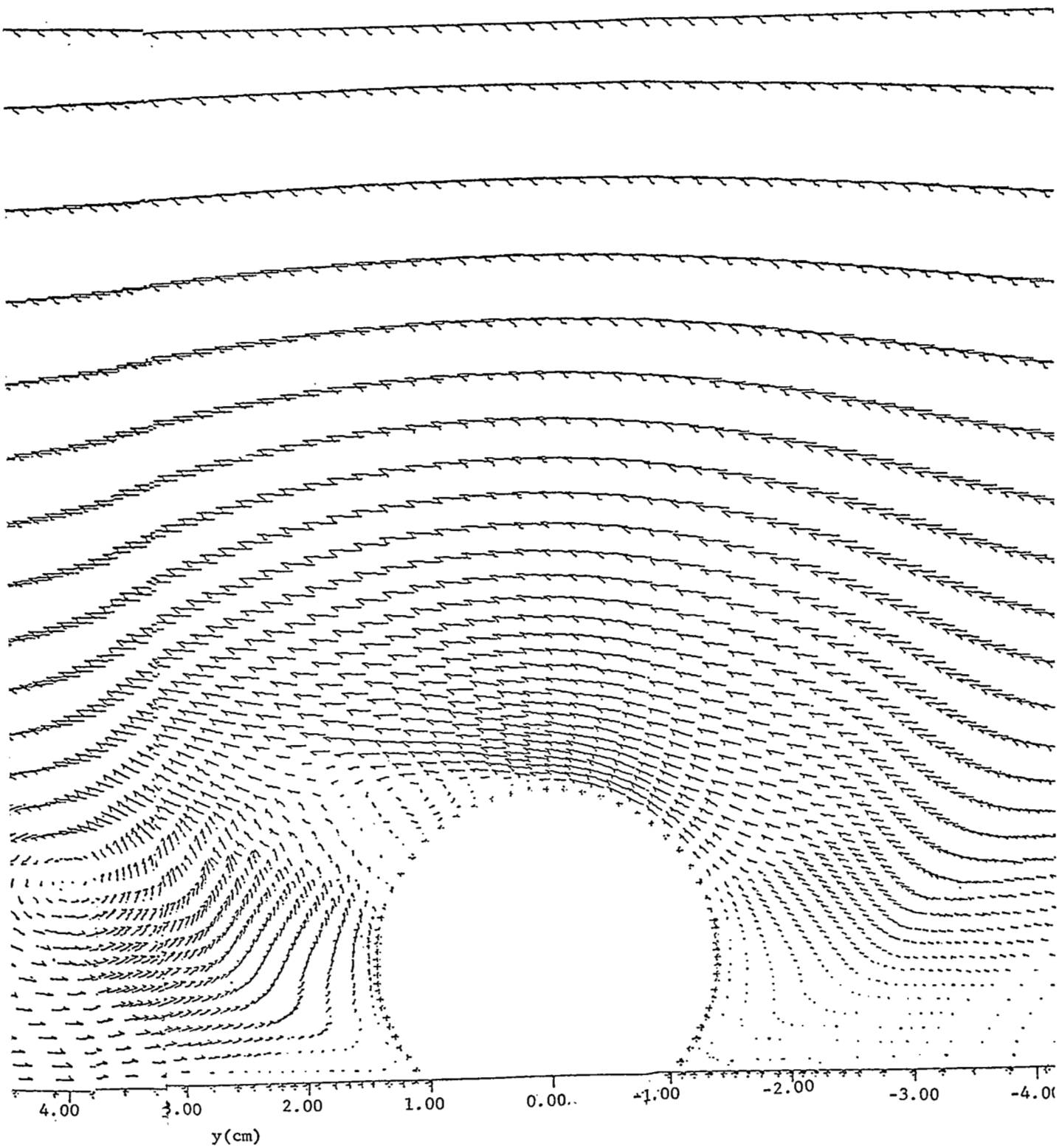
4.00
3.00
2.00
1.00
0.00
-1.00
-2.00
-3.00
-4.0(
y(cm)

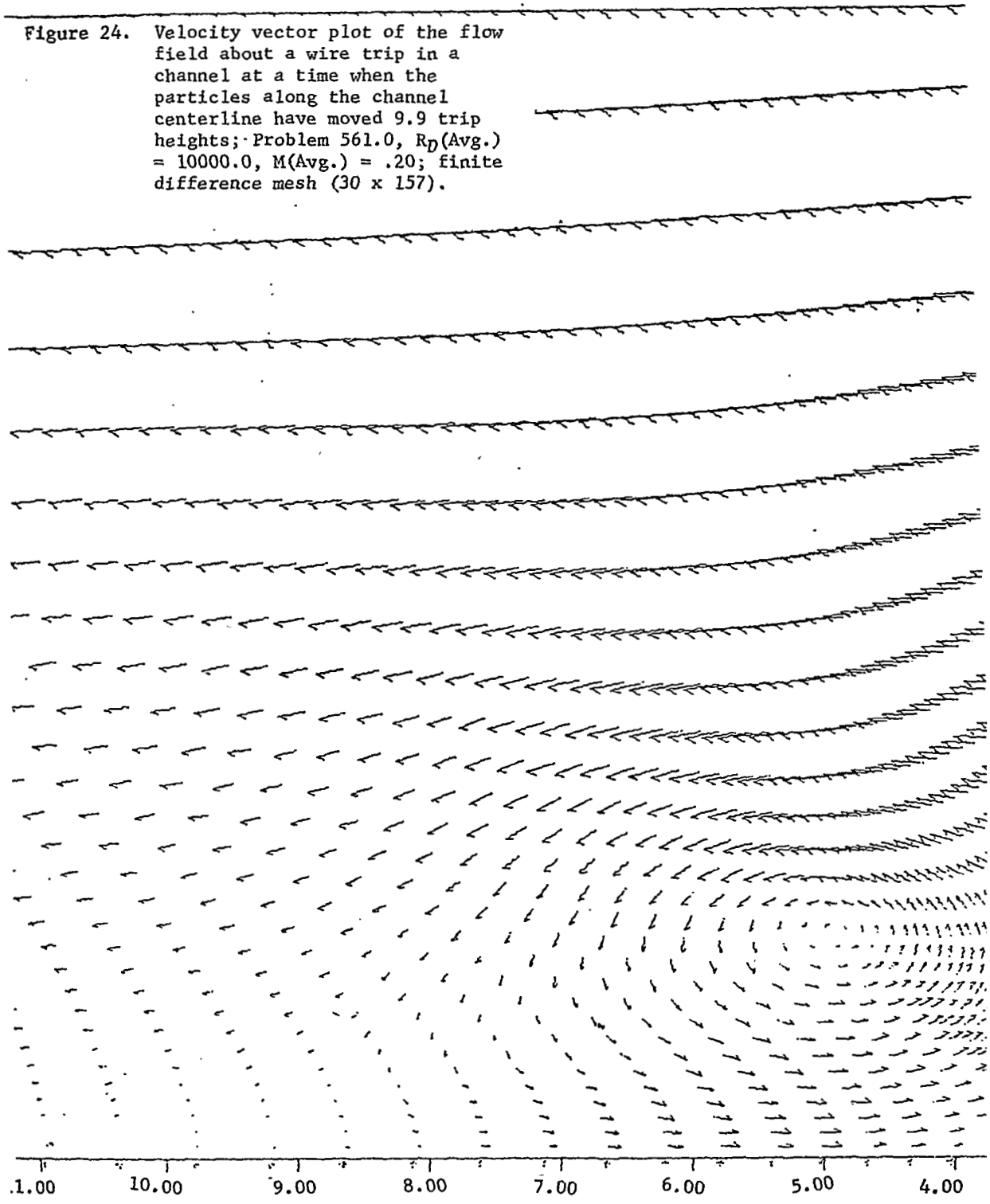

Figure 24. Velocity vector plot of the flow field about a wire trip in a channel at a time when the particles along the channel centerline have moved 9.9 trip heights; Problem 561.0, R_D(Avg.) = 10000.0, M(Avg.) = .20; finite difference mesh (30 x 157).

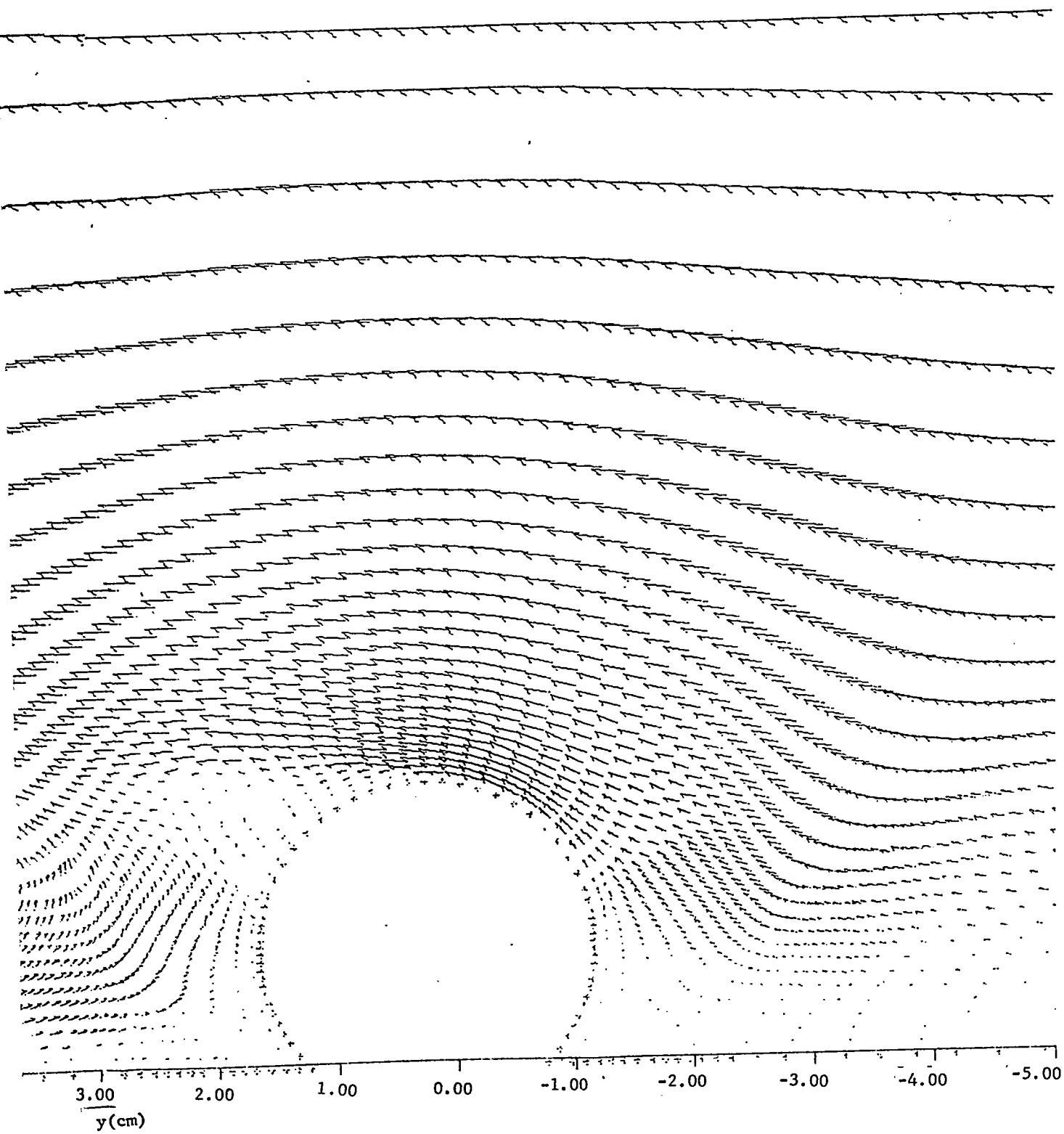
3.00
2.00
1.00
0.00
-1.00
-2.00
-3.00
-4.00
-5.00
y(cm)

a. Mean motion and fluctuations

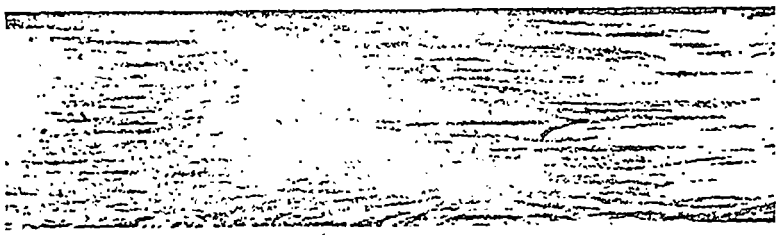

Fig. 25 a. Camera velocity 12·15 cm/sec

Fig. 25 b. Camera velocity 20 cm/sec

Fig. 25 c. Camera velocity 25 cm/sec

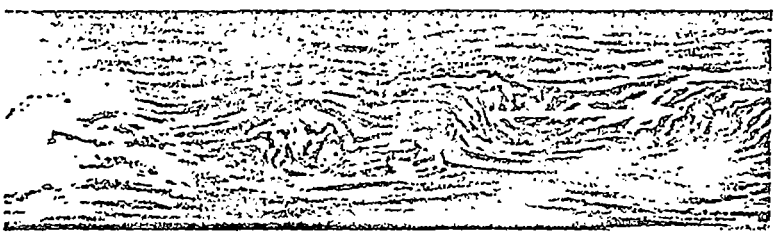

Fig. 25 d. Camera velocity 27·6 cm/sec

Figure 25 a,b,c,d. Turbulent flow in a water channel 6 cm wide, photographed with varying camera speeds. Photographs taken by Nikuradse[24] and published by Tollmien

REFERENCES

1. Trulio, J.G., "Theory and Structure of the AFTON Codes," Technical Report No. AFWL-TR-66-19 (1966)

2. Schlichting, H., "Boundary Layer Theory," McGraw-Hill Book Company, 1960, p. 116 and p. 212.

3. Trulio, J.G., and Walitt, L., "Numerical Calculations of Viscous Compressible Fluid Flow," Applied Theory Report No. ATR-68-5-1, 1968, to be published as a NASA contractor report.

4. Reference 2, p. 396.

5. Schlichting, H., "Boundary Layer Theory," McGraw-Hill Book Company, 1960, p. 67.

6. Hayes, W. D., and Probstein, R. F., "Hypersonic Flow Theory," Academic Press, 1960, p. 482 and p. 485.

7. Trulio, J.G., Niles, W. J. Carr, W. E., and Rentfrow, R.L., "Calculation of Two-Dimensional Turbulent Flow Fields," NASA CR-430 (1966).

8. Reference 5, p. 212.

9. Reference 5, p. 168.

10. Reference 5, p. 116.

11. Kistler, A.L., "Fluctuating Wall Pressure Under a Separated Supersonic Flow," Journal of the Acoustical Society of America, Vol. 36, No. 3, March 1964, pp. 543-550.

12. von Neumann, J., and Richtmyer, R.D., "A Method for the Numerical Solution of Hydrodynamic Shocks," Journal of Applied Physics, Vol. 21, March 1950.

13. Reference 5, p. 571.

14. Reference 5, p. 347.

15. Liepmann, H. W., and Roshko, A., "Elements of Gas Dynamics," Wiley (1962) pp. 340-342.

16. Stewartson, K., "Correlated Incompressible and Compressible Boundary Layers," Proc. Roy. Soc. London A200, 1950, pp. 84-100.

17. Reference 15, p. 87

18. Schubauer, G. G., and Skramstad, H. K., "Laminar Boundary Layer Oscillations and Stability of Laminar Flow," NACA Report No. 909(1948).

REFERENCES (continued)

19. Mack, L. M., "The Stability of the Compressible Laminar Boundary Layer According to a Direct Numerical Solution," Proceedings of a Specialists' Meeting, sponsored by the AGARD Fluid Mechanics Panel, held in Naples, Italy, 10-14 May 1965.

20. Schlichting, H., "Boundary Layer Theory," McGraw-Hill Book Company, 1960, p. 400.

21. Reference 20, p. 446.

22. Reference 20, p. 67.

23. Milne-Thomson, L. M., "Theoretical Hydrodynamics," Macmillan Company, 1965, p. 174.

24. Reference 16, p. 458.

25. Nikuradse, J., "Kinematographische Aufrahme eines Turbulenten Stromung," Zamin 9, 495 (1929).

NASA-Langley, 1970 —— 12